Published in final edited form as:
J Comp Neurol. 2014 April 15; 522(6): 1411–1443. doi:10.1002/cne.23521.

The RNA binding protein RBPMS is a selective marker of ganglion cells in the mammalian retina

Allen R. Rodriguez[1], **Luis Pérez de Sevilla Müller**[1], and **Nicholas C. Brecha**[1,2,3,4,5]

[1]Department of Neurobiology, David Geffen School of Medicine at Los Angeles, University of California at Los Angeles, Los Angeles, California 90095-1763

[2]Department of Medicine, David Geffen School of Medicine at Los Angeles, University of California at Los Angeles, Los Angeles, California 90095-1763

[3]Jules Stein Eye Institute, David Geffen School of Medicine at Los Angeles, University of California at Los Angeles, Los Angeles, California 90095-1763

[4]CURE Digestive Diseases Research Center, David Geffen School of Medicine at Los Angeles, University of California at Los Angeles, Los Angeles, California 90095-1763

[5]Veterans Administration Greater Los Angeles Health System, Los Angeles, California 90073

Abstract

There are few neurochemical markers that reliably identify retinal ganglion cells (RGCs), which are a heterogeneous population of cells that integrate and transmit the visual signal from the retina to the central visual nuclei. We have developed and characterized a new set of affinity purified guinea pig and rabbit antibodies against RNA-binding protein with multiple splicing (RBPMS). On Western blots these antibodies recognize a single band at ~24 kDa, corresponding to RBPMS, and they strongly label RGC and displaced RGC (dRGC) somata in mouse, rat, guinea pig, rabbit and monkey retina. RBPMS immunoreactive cells and RGCs identified by other techniques have a similar range of somal diameters and areas. The density of RBPMS cells in mouse and rat retina is comparable to earlier semi-quantitative estimates of RGCs. RBPMS is mainly expressed in medium and large DAPI-, DRAQ5-, NeuroTrace- and NeuN-stained cells in the ganglion cell layer (GCL), and RBPMS is not expressed in syntaxin (HPC-1) immunoreactive cells in the inner nuclear layer (INL) and GCL, consistent with their identity as RGCs, and not displaced amacrine cells. In mouse and rat retina, most RBPMS cells are lost following optic nerve crush or transection at three weeks, and all Brn3a, SMI-32 and melanopsin immunoreactive RGCs also express RBPMS immunoreactivity. RBPMS immunoreactivity is localized to CFP-fluorescent RGCs in the B6.Cg-Tg(Thy1-CFP)23Jrs/J mouse line. These findings show that antibodies against RBPMS are robust reagents that exclusively identify RGCs and dRGCs in multiple mammalian species, and they will be especially useful for quantification of RGCs.

Corresponding Author: Nicholas Brecha, PhD, Department of Neurobiology, David Geffen School of Medicine at Los Angeles, UCLA, 10833 Le Conte Ave., Los Angeles, California 90095-1763, nbrecha@ucla.edu, Phone: 310-825-6758, Fax: 310-825-2224.

Conflict of interest statement
The authors declare no competing financial interests.

Contributions
N.C.B. conceived the project and A.R.R., L.P.S.M. and N.C.B. designed the experiments; A.R.R. performed the experiments and analyzed the data; A.R.R., L.P.S.M. and N.C.B. wrote the paper; L.P.S.M. and N.C.B. supervised the project.

Keywords

(3, 6): RNA-binding protein; transcription factor; melanopsin; SMI-32; ganglion cell; amacrine cell

Introduction

The ganglion cell layer (GCL) consists of a heterogeneous group of neurons, including retinal ganglion cells (RGCs) and displaced amacrine cells, as well as astrocytes, microglia and vascular endothelial cells. RGCs consist of about 21 morphologically distinct types in the mammalian retina and they project to multiple targets in the central nervous system (CNS) (Rockhill et al., 2002; Sun et al., 2002a; b; Badea and Nathans, 2004; Kong et al., 2005; Coombs et al., 2006; Völgyi et al., 2009). Displaced amacrine cells, which also consist of multiple morphological types, constitute a large percentage and in some species the majority of neurons in the GCL (Hughes and Wieniawa-Narkiewicz, 1980; Perry and Walker, 1980; Wässle et al., 1987; Badea and Nathans, 2004; Pérez de Sevilla Müller et al., 2007). For instance, in mouse (Jeon et al., 1998; Pang and Wu, 2011), rat (Perry, 1981) and rabbit (Vaney, 1980) retina, displaced amacrine cells constitute about 55–56%, 40–50% and 30% of the neurons in the GCL, respectively. In addition, there are displaced RGCs (dRGCs) in the inner nuclear layer (INL) at the inner plexiform layer (IPL) border, and they are reported to constitute about 2 – 3% of the total RGC population in mouse (Dräger and Olsen, 1981; Pang and Wu, 2011) and rat (Liu and Jen, 1986) retina.

Over the past few decades, numerous efforts have focused on developing methods to reliably distinguish between RGCs and displaced amacrine cells. RGCs and displaced amacrine cells can be broadly divided into a medium and large size group, and into a small size group, respectively. RGC somata have more prominent Nissl substance and a centrally located nucleus, compared to amacrine cell somata that have a condensed nucleus. These morphological characteristics have provided the basis for distinguishing between these two cell types. However, it is often difficult to distinguish unequivocally between small RGCs and large displaced amacrine cells, because of overlap in their somal sizes, and similarities in their cytological features (Vaney, 1980; Perry, 1981; Pérez de Sevilla Müller et al., 2007). A classical approach to distinguish between ganglion and displaced amacrine cells is to use the retrograde transport of neuronal tracers, such as horseradish peroxidase (HRP) or fluorescent dyes, such as Fluorogold, or the carbocyanine dye, 1,18-dioctadecyl-3,3,38,38-tetramethylindocarbocyanine perchlorate (DiI) to identify RGCs (Bunt et al., 1974; Berkelaar et al., 1994; Huxlin and Goodchild, 1997; Pang and Wu, 2011). This procedure requires injections of the tracer into central visual targets or its application to the optic nerve. The retrograde transport of neuronal tracers has the advantage of identifying the RGCs types that project to a particular target in the CNS. However, there are several drawbacks of using this approach, including damage to RGC axons, and variable uptake and transport of the tracer as well as difficulty in adequately labeling multiple RGC central targets, which potentially results in an incomplete labeling of the RGC population.

An alternative is to use antibodies, dyes or fluorescent reporters introduced by biolistic delivery (particle bombardment) or genetic approaches to identify displaced amacrine and ganglion cells. Displaced amacrine cells express syntaxin 1 (HPC-1), GABA and GAD immunoreactivity, and these neurochemical attributes are often used to define this cell population (Barnstable et al., 1985; Wässle et al., 1987; Koontz et al., 1993; Kao and Sterling, 2006; Pérez de Sevilla Müller et al., 2007). Immunohistochemical approaches to identify RGCs have used several different antibodies, including those directed to NeuN, Thy1 and substance P, but these often immunostain a subgroup of RGCs or

immunoreactivity is also expressed in other retinal cells, including displaced amacrine cells (Barnstable and Dräger, 1984; Perry and Cowey, 1984; Brecha et al., 1987; Mullen et al., 1992; Buckingham et al., 2008; Johansson et al., 2010). Biolistic delivery of DiI and genetic approaches with reporters have been used to identify and characterize individual ganglion cell types (Gan et al., 2000; Rockhill et al., 2002; Badea and Nathans, 2004; Huberman et al., 2008; Kim et al., 2008; Munch et al., 2009). In addition, several transgenic mouse lines, generated using the Thy1 promoter driving fluorescent reporter expression, contain a high number of labeled RGCs, but not all of the RGCs express the reporter at detectable levels. In addition, bipolar, amacrine and Müller cells also express the fluorescent reporter (Feng et al., 2000). There is a good understanding of individual RGC types, however quantitative studies of the entire RGC population have proven to be problematic, since these markers fail to selectively identify all RGCs.

Transcription factors, including Brn3 (*Pou4f*), Isl1 and Isl2, as well as RNA-binding proteins that are specific to RGCs have been identified in the retina, and some of them appear to be excellent markers for RGCs (Xiang et al., 1995; Piri et al., 2006; Elshatory et al., 2007; Kwong et al., 2010). A member of the RRM (RNA recognition motif) family of RNA-binding proteins, RNA-binding protein with multiple splicing (RBPMS) and its paralogue, *RBPMS2* (*hermes*) (Shimamoto et al., 1996; Gerber et al., 1999) are expressed in rat RGCs (Piri et al., 2006; Kwong et al., 2010). However, it is not fully established if RBPMS is also expressed in RGCs of other commonly used retinal model species, and whether RBPMS is expressed by dRGCs. In this study we have developed high titer, affinity purified polyclonal antibodies against RBPMS that detect on Western blots a band at ~ 24 kDa corresponding to RBPMS. Furthermore, RBPMS is mainly expressed in medium and large cells in the GCL, and a few cells in the INL at the IPL border of the mouse, rat, guinea pig, rabbit and monkey retina. In mouse and rat retina, RBPMS is likely to be expressed by the entire RGC population based on their distribution, size and number in the GCL and INL, and their loss after optic nerve crush or transection. Taken together, these findings indicate that RBPMS will be a highly useful marker for identifying RGCs in multiple mammalian species commonly used for experimental studies.

Materials and Methods

Animals

Adult C57BL/6, B6.Cg-Tg(Thy1-CFP)23Jrs/J (Feng et al., 2000) (20–30 g; Jackson Laboratory, Bar Harbor, ME), $Cx36^{-/-}$ (C57BL6/129SvEv hybrid) (Deans et al., 2002) mice, adult Sprague-Dawley rats (150–250 g), adult Hartley guinea pigs (CRL 051; Charles River, Wilmington, MA), adult New Zealand white rabbits (CRL 052; Charles River), and adult female and male macaque monkeys (*Macaca mulatta*) from Oregon Health and Science University (OSHU and UCLA), were used for these studies. All experiments were performed in accordance with the guidelines and policies for the welfare of experimental animals established by the U.S. Public Health Service Policy on Human Care and Use of Laboratory Animals (2002) and the UCLA Animal Research Committee.

Optic Nerve Crush and Transection

Adult C57BL/6 mice and Sprague-Dawley rats were anesthetized by isofluorane (3–5%) in oxygen (1.5 L/min). The canthus was cut, the tissue surrounding the optic nerve was dissected and the nerve was exposed. The mouse optic nerve was crushed about 1 mm posterior to the globe using reverse-action forceps for 15 seconds. The rat optic nerve sheath was incised longitudinally to expose the optic nerve axons. A complete transection of the optic nerve was made 2 mm posterior from the globe with surgical scissors without damage to the adjacent blood supply. The mice and rats were euthanized 21 days after optic nerve

crush or transection for the immunohistochemical studies, and a rat was euthanized 56 days after optic nerve transection for the Western blot studies.

Tissue preparation

Mice and rats were deeply anesthetized with 1–3% isofluorane (IsoFlo, Abbott Laboratories, North Chicago, IL). The mice were euthanized by cervical dislocation and the rats were euthanized by decapitation. Guinea pigs and rabbits were euthanized by an overdose of pentobarbital (100 mg/kg). The monkeys were euthanized with Euthasol (Virbac Corporation, Fort Worth, Texas) for other experimental procedures following sedation, and the retinas were collected and provided by OSHU and UCLA laboratory services. Mouse, rat, guinea pig and rabbit eyes were enucleated, and the anterior chamber and lens were removed.

Immunohistochemistry studies—The eyecups were fixed in 4% paraformaldehyde (PFA) in 0.1 M phosphate buffer (PB), pH 7.4, for 15–60 minutes and stored in 30% sucrose in 0.1 M PB overnight at 4°C. The monkey retina (UC1) from UCLA was fixed 30 minutes in 4% PFA and stored in 0.1 M PB at 4°C and the monkey retina from OSHU was fixed for 60 minutes in 4% PFA and stored in 30% sucrose in PB saline, and shipped to UCLA. For cryostat sections, the eyecup or isolated retina were sectioned vertically at 12 μm using a Leica CM3050S cryostat (Leica Microsystems, Buffalo Grove, IL) and collected onto gelatin-coated slides and stored frozen until immunohistochemistry processing. For whole-mounted retinas, the retina was separated from the sclera and mounted photoreceptor side down on black filter paper (EMD Millipore, Billerica, MA). Retinas were fixed in 4% PFA in 0.1 M PB for 15 minutes, and transferred to the blocking solution as described above for 12–16 hours overnight at 4°C before immunohistochemistry processing.

Western blot studies—C57BL/6 mouse and Sprague-Dawley rat retinas were isolated and placed immediately in 1.5 M Tris-HCl, 0.5 M EDTA, 0.5 M EGTA, and 20% Triton-X in dH_2O on dry ice. Cell lysis buffer also contained 10 μl/ml Halt Protease Inhibitor and 10 μl/ml Halt Phosphatase Inhibitor cocktails (Thermo Fisher Scientific, Waltham, MA). Samples were homogenized for 2 minutes and incubated on ice for 20 minutes to lyse cells. After centrifugation (20,100 *g*; 30 minutes at 4°C), the supernatant fractions were removed and the protein content of the samples was determined by using a NanoDrop Spectrophotometer (Thermo Fisher Scientific). Protein samples were diluted in Laemmli sample buffer containing beta-mercaptoethanol, pH 6.8 and samples were boiled for 10 minutes before loading onto the gel.

Antibody characterization (Table 1)

RBPMS antibodies—Guinea pig (4 animals; 15029–15032) and rabbit (2 animals; 15027, 15028) polyclonal antibodies were generated against the N-terminus of the RBPMS polypeptide ($RBPMS_{4-24}$; GGKAEKENTPSEANLQEEEVR) by a commercial vendor (ProSci Inc., Poway, CA). The RBPMS polypeptide was conjugated to keyhole limpet hemocyanin (KLH) via an additional N-terminal cysteine. The first immunization used the RBPMS polypeptide-KLH immunogen with complete Freund's adjuvant and subsequent immunizations used incomplete Freund's adjuvant. Subcutaneous injections of the RBPMS polypeptide-KLH immunogen occurred at two-week intervals, and plasma was collected 7 and 14 days after the immunization. Sera were tested for specific immunostaining with rat and mouse retina sections, and all bleeds were affinity purified using a RBPMS polypeptide affinity column (ProSci, Inc). Antibodies were eluted from the column with 100 mM glycine buffer pH 2.5, neutralized by 1 M Tris pH 9.5, dialyzed, and concentrated by Centriprep centrifugal filter units with Ultracel-30 membranes (EMD Millipore).

The specificity of the affinity purified guinea pig (GP15029) and rabbit (RB15027) antibodies was tested by Western blotting and immunohistochemistry. The guinea pig and rabbit antibodies recognized a single band at ~24 kDa close to the predicted molecular size of RBPMS (http://www.uniprot.org/uniprot/Q93062) on Western blots of HEK293T cell lysates transfected with a Myc-DDK-tagged-human RBPMS (LY425258; OriGene Technologies, Inc., Rockville, MD), and of mouse and rat retinal extracts. The same antibodies also robustly immunostained cells in the GCL of the mouse, rat, guinea pig, rabbit and monkey retina. To evaluate the specificity of the RBPMS immunostaining, a preabsorption control was performed with the guinea pig (GP15029) and rabbit (RB15027) antibodies used in this study. Briefly, the RBPMS antibodies were diluted in 0.1 M PB containing 0.5% Triton X-100 and mixed with the RBPMS polypeptide at a final concentration of 1 μg/ml for two hours at room temperature. No RBPMS immunostaining was present in sections incubated with the preabsorbed rabbit or guinea pig RBPMS antibodies.

Brn3a antibody—A mouse monoclonal antibody (MAB1585 clone 5A3.2; Millipore) was generated against the POU-domain (amino acids 186–224) of Brn3a fused to the T7 gene 10 protein. The antibody specifically recognizes Brn3a, with no reactivity to Brn3b or Brn3c by Western blots (manufacturer's data sheet). In addition, no Brn3a immunoreactivity was observed in Brn3a$^{-/-}$ mouse mutants (manufacturer's data sheet). The mouse monoclonal antibody also immunostains RGCs in the mouse and rat retina (Liu et al., 2009), and it has been used to isolate human RGCs (Zhang et al., 2010).

GABA antibody—The rabbit polyclonal antibody (A2052; Sigma-Aldrich, St. Louis, MO) against synthetic GABA conjugated to BSA shows positive immunoreactivity with GABA, and GABA-KLH in a dot blot assay, and no cross reactivity with BSA (manufacturer's data sheet). The antibody has been used extensively for identifying GABA-containing neurons in the rodent CNS (Ito et al., 2007; Panzanelli et al., 2007; Wolansky et al., 2007) including amacrine cells in the mouse retina (Dedek et al., 2009; Haverkamp et al., 2009; Pérez de Sevilla Müller et al., 2010b).

Glycine antibody—A rat polyclonal antibody (IG1002; ImmunoSolution, Queensland, Australia) to glycine was raised to a PFA conjugate of glycine and thyroglobulin (Pow et al., 1995). The glycine antibody reacts with glycine-BSA conjugates in dot blot assays and antibody specificity was shown by elimination of the immunoreactivity using the amino acid-PFA-thyroglobulin conjugate used to immunize the animals (Pow et al., 1995). In the retina, this glycine antibody mainly immunostains amacrine cells in rats, guinea pigs and rabbits (Pow et al., 1995; Menger et al., 1998; Pow and Hendrickson, 1999).

Melanopsin antibody—A rabbit polyclonal antibody (UF006; Advanced Targeting Systems, San Diego, CA) to the N-terminus of mouse melanopsin was raised against a synthetic polypeptide consisting of the 15 N-terminal amino acids of mouse melanopsin with an additional C-terminal cysteine (MDSPSGPRVLSSLTQC) conjugated to KLH (Panda et al., 2002). Specificity of this antibody was been confirmed in control studies showing a loss of immunostaining by preabsorption with the N-terminal melanopsin polypeptide and by the lack of immunoreactivity in the retinas of Opn4$^{-/-}$ mice (Panda et al., 2002). This antibody has been reported to immunolabel the M1, M2 and M3 ipRGC subtypes (Berson et al., 2010).

Melanopsin antibody—A rabbit polyclonal antibody (PA-781; Thermo Scientific) to the C-terminus of rat melanopsin was raised against a synthetic peptide of rat melanopsin$_{455\text{-}474}$ [E(455)-QKSKTPKTKRHLPSLDRRM-M(474)]. Specificity of this antibody has been

shown by immunostaining of the tdTomato-fluorescent cells in the melanopsin:tdTomato mouse retina (Do et al., 2009). This antibody has been reported to immunolabel M1 ipRGCs (Baver et al., 2008; Pérez de Sevilla Müller et al., 2010b).

NeuN antibody—A mouse monoclonal antibody (MAB377; Millipore) was raised against purified cell nuclei from mouse brain. This antibody specifically recognizes the nuclei of most neuronal cell types in the adult mammalian brain (Mullen et al., 1992). Western blot of rat brain showed two or three bands in the 46–48 kDa range, which are likely to be multiple phosphorylated forms of the same antigen (Lind et al., 2005). This antibody immunostains RGCs and amacrine cells in the mouse and pig retina (Buckingham et al., 2008; Raymond et al., 2008; Johansson et al., 2010).

SMI-32 antibody—A mouse monoclonal antibody (SMI32 Lot#17; Sternberger Monoclonals Incorporated, Luthersville, MD), was raised against the non-phosphorylated epitopes on the medium and heavy molecular weight subunits of neurofilament H (NFH) in immunoblots of mammalian brainstem and spinal cord tissue [(Sternberger and Sternberger, 1983); manufacturer's datasheet]. On conventional immunoblots, the SMI-32 antibody identifies two bands (200 and 180 kDa), which merge into a single NFH line on two-dimensional blots (Sternberger and Sternberger, 1983; Goldstein et al., 1987). The SMI-32 antibody immunostains neuronal cell bodies, dendrites and thick axons in both the central and peripheral nervous systems (Sternberger and Sternberger, 1983) whereas other cells and tissues are not immunostained (manufacturer's datasheet). In the retina, this antibody immunostains the cytoskeleton of medium and large ganglion cells, as well as ganglion cell axons of mouse, rat and cat retina (Wässle et al., 1981; Lin et al., 2004; Coombs et al., 2006).

Syntaxin 1—A mouse monoclonal antibody (clone HPC-1, S0664; Sigma) was raised against a synaptosomal plasma membrane fraction from adult rat hippocampus (Barnstable et al., 1985). The syntaxin 1 antibody immunolabels a single band near 36 kD on Western blots of mouse brain and retina, and detects the synaptic protein, syntaxin 1a (Inoue et al., 1992). The syntaxin 1 antibody immunostains amacrine and horizontal cell bodies and processes (Barnstable et al., 1985; Hirano et al., 2005; Sherry et al., 2006).

Cellular markers

DAPI (4′,6-Diamidino-2-phenylindole dihydrochloride) and DRAQ5 (1,5-bis {[2-(di-methylamino) ethyl] amino}-4,8-dihydroxyanthracene-9,10-dione) are cell permeable, blue and far-red fluorescent DNA dyes, which also bind RNA (Vector Laboratories and AbCam; manufacturer's datasheet). NeuroTrace is a cell permeable, red fluorescent stain selective for Nissl substance (mRNA and rough endoplasmic reticulum (Invitrogen; manufacturer's datasheet).

Immunohistochemistry

Immunohistochemical labeling was performed using an indirect immunofluorescence method (Hirano et al., 2005). Retinal sections were incubated in a blocking solution of 10% normal goat serum (NGS), 1% bovine serum albumin (BSA) and 0.5% Triton X-100 in 0.1 M PB for 1 hour at room temperature. The blocking solution was removed and the sections were immediately incubated with the primary antibody (see Table 1) in a primary antibody solution (3% NGS, 1% BSA, 0.05% sodium azide and 0.5% Triton X-100 in 0.1 M PB, pH 7.4) for 12–16 hours at 4°C in a humidified chamber. Retinal sections were rinsed three times for 10 minutes with 0.1 M PB to remove excess primary antibody and the corresponding secondary antibody was applied for 1 hour at room temperature in the dark. Secondary antibodies used in this study were Alexa-488 and -568 goat anti-guinea pig IgG,

Alexa-488 goat anti-mouse IgG, Alexa-488 goat anti-rat IgG, and Alexa-488 goat anti-rabbit IgG at 1:1000 (Invitrogen, Carlsbad, CA). After a final wash of three times 10 minutes in 0.1 M PB, the retinal sections were mounted using Aqua Poly/Mount (Polysciences, Inc., Warrington, PA). As a negative control, the omission of the primary antibodies in the single and double labeling studies was conducted to evaluate nonspecific binding of the secondary antibody.

Whole-mounted retinas were incubated with the primary antibodies for single, double and triple label immunostaining for 5 to 7 days at 4°C. Retinas were rinsed three times for 30 minutes with 0.1 M PB and incubated with the corresponding secondary antibodies conjugated with Alexa 568, Alexa 488 or Alexa 633 at 1:1000 (Invitrogen) for 12–16 h at 4°C. After a final wash of three times in 0.1 M PB for 30 minutes, the whole-mounted retinas were placed on a microscope slide with the GCL up and cover slipped with Aqua Poly/Mount or Vectashield (Vector Laboratories, Burlingame, CA).

Some immunostained mouse, rat and guinea pig whole-mounted retinas, and a section of the monkey whole-mounted retina (UC1) were also incubated in DAPI (H1200; Vector Laboratories), DRAQ5 (ab108410; Abcam, Cambridge, MA) or NeuroTrace 530/615 (Invitrogen N-21482; Life Technologies, Grand Island, NY), fluorescent cellular makers. Retinas were cover slipped in a mounting medium containing DAPI or incubated in DRAQ5 at 1:1000 in 0.1 M PB for 5 minutes, after the completion of the secondary antibody incubation, and subsequently cover slipped. NeuroTrace at 1:100 was included in the secondary antibody incubation.

Western Blotting

Western blotting was used to characterize the specificity of the RBPMS antibodies and to determine the presence of RBPMS in mouse and rat retina. Cell lysates (10 μg) from HEK293T cells transfected with human RBPMS cDNA was loaded alongside a lysate (10 μg) of non-transfected HEK293T cells (negative control) (OriGene Technologies) and assayed by a Western blot. Total protein (25 μg) from mouse and rat retina, and a rat retina collected at 56 days after optic nerve transection were also assayed by a Western blot. Prestained marker proteins were used as molecular mass standards (Bio-Rad, Hercules, CA). Proteins were fractionated (200V for 30 minutes) by 10% Tris-glycine SDS-Page using Mini-Protean TGX Gel System (Bio-Rad), rinsed briefly, and then transferred at 400 mA for 90 minutes at 4°C. Blots were blocked for 1 hour at room temperature in a non-mammalian Odyssey Blocker (Bio-Rad), and incubated with guinea pig or rabbit RBPMS antibodies (see Table 1) at 1:1500 overnight on a shaker at 4°C. Blots were rinsed in a solution containing 0.1 M PB, 0.154 M NaCl, and 0.05% Tween 20 (v/v) at pH 7.4 for 30 minutes, and incubated in donkey anti-rabbit IgG-conjugated IRDye 800CW or donkey anti-guinea pig IgG-conjugated IRDye 680RD (LI-COR, Lincoln, NE) diluted at 1:10,000 in blocking buffer for 1 hour at room temperature. The blots were washed and immediately imaged by using the LI-COR Odyssey Infrared Imaging System and evaluated by using proprietary software.

Fluorescent Image Acquisition

Immunostaining was examined using a Zeiss Laser Scanning Microscope 510 META or 710 (Carl Zeiss, Thornwood, NY) with a Zeiss Plan-Apochromat 20x/.08 NA, Zeiss Plan-Neofluar 25x/ 0.8 NA water, Zeiss C-Apochromat 40x/ 1.2 NA water or a Zeiss Plan-Apochromat 63x/ 1.4 NA oil objective. Digital images were collected at a resolution of 1024 × 1024 or 2048 × 2048 pixels. Images are presented either as a single image scan or as projections of 2–20 image stacks (z-axis step size 0.34 to 1.1 μm). Confocal images were analyzed using the Zeiss LSM 510 proprietary software (version 3.2). Intensity levels and

contrast of the final images were adjusted in Adobe Photoshop CS2 v.9.02 (Adobe Systems, San Jose, CA).

Semi-Quantification of RBPMS somal size and density

Digital images were made of RBPMS-immunoreactive somata from whole-mounted retinas in all retinal quadrants (superior, temporal, inferior, nasal) at different retinal eccentricities. Sample retinal fields measured 250 × 250 μm^2 and viewed at 20x or 25x with a 0.7 to 1.0 magnification factor. Somal cell number and diameters were determined from digital images that were preprocessed to set intensity and background levels by enhancing contrast, subtracting background and applying a Gaussian blur using the Fiji plug-in for ImageJ (Schindelin et al., 2012). RBPMS-immunoreactive cell bodies were identified using an object-recognition macro written in-house. Objects under 20 μm^2 were excluded as background. Each image was visually inspected after processing and objects not corresponding to RBPMS somata were excluded from analysis.

Somal diameter and area—RBPMS cell diameter and area were determined using Fiji's object area and Feret diameter calculations. Feret diameter was calculated as the longest distance between any two points on an object's perimeter, also known as the maximum caliper. Somal area was calculated by converting the pixel dimensions of an object into the μm scale of the image. Cell sizes from multiple images were grouped by species and retinal position, and automatic binning was used to construct histograms using SigmaPlot (Systat Software, Inc., San Jose, CA) or fit with a normal curve in R-Studio for R (http://www.r-project.org/). Somal diameters were combined in all sample fields to determine somal size range, as well as average and median somal size for mouse, rat, guinea pig, rabbit and monkey retina. In addition, in mouse and rat retina, somal size distribution was determined in central, mid-peripheral and peripheral retinal regions.

Somal number—RBPMS cell number and density (cells/mm^2) were determined manually using the cell counter in ImageJ. Cell number from multiple images were grouped by retinal eccentricity, and statistics were calculated using SigmaPlot (Systat Software, Inc.). In optic nerve crushed and transected rat retinas, the percent cell loss was defined as the density of cells in the GCL of the injured retina divided by the density of cells in the GCL of the non-operated retina, subtracted from 1. All cell statistics are presented as the mean ± SD

Mouse and rat retinas—Somal diameter size and number were determined in a minimum of four adjacent sample fields at each retinal location that were separated by 0.5 mm intervals from the optic nerve head to the retinal margin in each retinal quadrant. These values were combined to determine the range and average RBPMS somal diameters, and for comparison of central and peripheral retinal regions. The density of RBPMS cells at each of the retinal locations were based on cell counts at the same retinal location across multiple retinas (N=6). Somal number was determined by finding the average cell number at each retinal location, then determining the average cell number at the same retinal eccentricity in all retinal quadrants. Finally, the average cell number at a particular retinal eccentricity was combined across multiple retinas.

For the mouse optic nerve crush and the rat optic nerve transection experiments, at least 4 sample fields at 12 locations, which were distributed to central and peripheral retinal regions and included all retinal quadrants, were evaluated for RBPMS cell number. For the RBPMS antibody and DAPI, DRAQ5, NeuroTrace and NeuN co-staining experiments, at least 1 sample field in 4 separate eccentricities approximately 2 mm from the center of the optic nerve were evaluated from all retinal quadrants. For the RBPMS and Brn3a, SMI-32 and

melanopsin co-localization experiments at least 1 sample field in 12 locations were evaluated from all retinal quadrants.

Guinea pig and rabbit retinas—Somal diameters were determined in a minimum of 1 sample field at 6 locations distributed to central and peripheral retinal regions from all retinal quadrants, and these values were combined to determine the range and average RBPMS somal diameters. The density of RBPMS cells were based on the cell counts from a sample field located in superior, temporal, inferior and nasal retinal regions of one or two retinas. Cell density values were not averaged across different retinas. For the RBPMS and NeuroTrace co-staining experiments in guinea pig retina, 2 sample fields 3 mm from the optic nerve was evaluated from 1 retinal quadrant.

Monkey retina (UC1)—a minimum of 4 sample fields at each location were evaluated in the temporal retina, which included the parafovea, and 3 sample fields in the peripheral inferior nasal retina were evaluated for RBPMS size and density. For the RBPMS, and the DRAQ5 or the NeuN co-staining experiments, at least 4 sample fields in 2 peripheral dorsal (> 7 mm from the optic nerve head) retinal locations were evaluated.

RESULTS

RBPMS and its paralogue, RBPMS2 were initially reported in the embryonic *Xenopus* GCL and in rat RGCs (Gerber et al., 1999; Piri et al., 2006; Kwong et al., 2010). Here we tested whether RBPMS is expressed in the retinas of mouse, rat, guinea pig, rabbit and monkey using newly developed guinea pig and rabbit polyclonal antibodies directed to the N-terminus of RBPMS.

Characterization of the RBPMS antibodies

Affinity purified polyclonal guinea pig (GP15029) and rabbit (RB15027) antibodies were generated to the N-terminus of the RBPMS polypeptide, $RBPMS_{4\text{-}24}$. $RBPMS_{4\text{-}24}$ is unique to RBPMS, and it shares amino acid sequence identity with RBPMS2 at $RBPMS_{4,\ 5\ \&\ 20\text{-}24}$ (http://www.uniprot.org/uniprot/Q93062). RBPMS is highly conserved among mammals and the sequence used for immunization is identical for mouse, rat, monkey and human, and 95% similar for guinea pig (NCBI Protein Bank, http://www.ncbi.nlm.nih.gov/protein). The guinea pig and rabbit antibodies detected a single band at ~24 kDa on Western blots of cell lysates from HEK293T cells transfected with human RBPMS cDNA (Figure 1, lanes 1 and 3) closely corresponding to the predicted molecular weight of RBPMS. No bands were detected in non-transfected HEK293T cell lysates (Figure 1, lanes 2 and 4).

Localization of RBPMS immunoreactivity in the mammalian retina

The presence of RBPMS in mouse and rat retinas was tested on Western blots with both the guinea pig and rabbit antibodies. As in the Western blots of RBPMS transfected HEK293T cells, a single band at ~24 kDa was detected in both mouse and rat retinal extracts (Figure 1, lanes 5, 6, 8 and 9). Furthermore, a weak immunostained band at ~24 kD was detected in a rat retinal extract collected 56 days after optic nerve transection (Figure 1, lanes 7 and 10).

Specific RBPMS immunoreactivity was mainly localized to medium to large diameter somata in the GCL (Figure 2), and to a few medium and large somata in the INL at the IPL border (Figure 2C). Some smaller diameter somata also contained RBPMS immunoreactivity. Robust immunostaining mainly occurred in the cell body, and strong immunostaining was present in the primary dendrites of larger diameter cells (Figure 3). Lower levels of immunostaining were in varicosities and thin dendrites in all laminae of the IPL. Immunostaining was mainly confined to the cytoplasm, although there was also weak

immunostaining of the nucleus. In addition, weak RBPMS immunostaining was seen in some ganglion cell axons in the nerve fiber layer (NFL) near the optic nerve head. Immunostaining was absent in photoreceptors, as well as horizontal, bipolar and amacrine cells, Müller cells and microglia.

Specific and robust RBPMS immunostaining was detected in the retinas of the mammalian species we evaluated with either the affinity purified guinea pig or rabbit polyclonal antibodies (Figure 2). RBPMS immunostaining was absent in retinal sections incubated in the affinity purified primary antibodies (GP15029 and RB15027), which had been pre-incubated with the RBPMS polypeptide used for generating the RBPMS antibodies (Figures 2 B, D, F, H, J and L). In a control study, using double labeling immunohistochemistry with both the guinea pig and rabbit antibodies, there was complete overlap of immunostained somata in a whole-mounted rat retina (data not shown).

RBPMS-immunoreactive cells in the GCL; somal size and density

The size and density of RBPMS-expressing somata were characterized using whole-mounted retinas from mouse (N=6 retinas), rat (N=6 retinas), guinea pig (N=3 retinas), rabbit (N=2 retinas) and macaque monkey (N=2 retinas) (Figures 4–7, and Table 2).

Somal size—RBPMS somal diameters in all retinal locations were combined to determine their range, as well as their average and median size. Overall, RBPMS-expressing somata ranged from about 9 to over 30 μm in diameter in mouse, rat, guinea pig, rabbit and monkey retina (Figure 5 and Table 3). The range of the middle 75% of the RBPMS cell diameters in the mouse and rat was 14.1 to 21.8 μm, and 13.1 to 20.8 μm, respectively. They averaged 17.9 ± 3.6 μm (n=1843) and 16.9 ± 3.5 μm (n=4526) in diameter in mouse and rat, respectively. RBPMS cells were smaller in central retina compared to peripheral retina (Figure 6 D, E, and Figure 7 D, E). In the mouse GCL, somal diameters averaged 17.1 ± 2.6 μm at 0.5 mm and 20.8 ± 4.1 μm at 2.0 mm from the optic nerve head (n = 500 cells for each group). In the rat GCL, somal diameters averaged 16.5 ± 3.3 μm at 0.5–1.0 mm and 18.7 ± 3.7 μm at ≥ 2.5 mm from the optic nerve head (n = 1000 cells each group). In guinea pig and rabbit, the range of the middle 75% of RBPMS cell diameters was 13.1 to 20.0 μm, and 12.8 to 19.1 μm, respectively. In the monkey retina (UC1), the range of the middle 75% of RBPMS cells in the sample of the temporal retina was 10.0 to 15.4 μm, and in the sample of the peripheral nasal retina, the range of the middle 75% of RBPMS cell diameters was 13.7 to 20.7 μm. The absolute range of RBPMS somal diameters as well as their average and median somal diameters are given in Tables 2 and 3.

In the mouse and rat retina, a small (0.2%) percentage of the RBPMS cells measured less than 10 μm in diameter. In the guinea pig, rabbit and monkey retina, RBPMS cells measuring less than 10 μm in diameter were very rare. In the retinas evaluated in this study, fewer than 4.0% of the RBPMS cells measured 25 μm or greater and there were very few RBPMS somata that were greater than 30 μm in diameter.

The frequency and distribution of RBPMS somal diameters and areas are similar, as expected (Figure 4). Somal areas are given to faciliate comparisons with some of the previous studies, which report the area of RGCs. Overall, the range and average RBPMS somal diameters and areas for the species evaluated in this study overlap the size of RGCs identified by other methods (Bunt et al., 1975; Robson and Holländer, 1984; Do-Nascimento et al., 1991; Sun et al., 2002a; b; Coombs et al., 2006; Pang and Wu, 2011) (Tables 2 and 3).

Somal density—RBPMS-immunoreactive cells were counted at different retinal locations (eccentricities) in all regions (superior, temporal, inferior, nasal) of the mouse, rat, guinea

pig and rabbit retinas, and in the temporal and inferior nasal region of one monkey retina (UC1).

The highest density of RBPMS cells was in the central region of the mouse, rat and guinea pig retina, the visual streak of the rabbit retina and in the parafovea region of the temporal monkey retina. The fovea was not present in the monkey retinal sample.

In both the mouse and rat retina, the highest density of RBPMS cells was located 0.5 mm from the optic nerve head. In mouse retina, average RBPMS cell density in the GCL at 1.0 and 2.5 mm from the center of the optic nerve head was 4890 ± 220 cells/mm^2 and 1847 ± 286 cells/mm^2, respectively (Figure 6 F). In the rat retina, average RBPMS cell density in the GCL at 1.0 and 4.0 mm from the center of the optic nerve head was 2938 ± 569 cells/mm^2 and 1362 ± 406 cells/mm^2, respectively (Figure 7 F).

RBPMS cell density in the GCL also varied across guinea pig and rabbit retinas, with the highest density in the central retina (2064 ± 23 cells/mm^2) of the guinea pig and the visual streak (3409 ± 135 cells/mm^2) of the rabbit. The lowest cell density in both species was in far peripheral retina with 210 cells/mm^2 in the guinea pig and 125 cells/mm^2 in the rabbit retina. In the monkey GCL, RBPMS-containing cells formed multiple rows in the parafovea and a single row in peripheral nasal and temporal regions. In mid-peripheral temporal retina, average RBPMS density was 2760 ± 548 cells/mm^2. In far peripheral inferior nasal retina, RBPMS cell density was 753 ± 145, 701 ± 151 and 523 ± 105 cells/mm^2 in three different locations. A regional distribution of RBPMS cell density was not determined for the guinea pig, rabbit or monkey retina because a small number of retinal locations and retinas were evaluated for each of these species.

Somal size and distribution of RBPMS-immunoreactive cells in the INL

The size and distribution of RBPMS-expressing somata in the INL were also characterized from whole-mounted retinas (Figure 8 and Table 2). In the INL, robust RBPMS immunostaining was mainly observed in medium, and a few small and large somata in the INL at the IPL border. RBPMS cells at the border of the INL were in all regions of every whole-mount preparation, and occasionally they were seen in the INL in vertical retinal sections. In addition, very few RBPMS cells were in the IPL of the mouse and rat retina. The infrequent occurrence of cells in the IPL and the relatively small number of vertically sectioned guinea pig, rabbit and monkey retinas did not allow us to determine if RBPMS cells were also in the IPL of these retinas.

Somal size—RBPMS cells in the INL ranged from about 8 to 27 μm in diameter in mouse, rat, guinea pig, rabbit and monkey retina (Figure 8, and Tables 2 and 4). In mouse and rat retina, the range of the middle 75% of the RBPMS cell diameters was 10.7 to 15.8 μm and 10.4 to 16.8 μm, respectively. Furthermore, in mouse and rat retina, the average RBPMS somal diameter was 13.0 ± 2.3 μm (n=237 cells) and 12.9 ± 3.0 μm (n=134 cells), respectively. For comparison, adjacent GABA-immunoreactive amacrine cell bodies were smaller and ranged from 6.5 to 12.9 μm in diameter in the mouse retina, with a mean diameter of 9.5 ± 1.3 μm (n=148). In the guinea pig INL, RBPMS cells ranged from 10.3 to 17.1 μm in diameter with a mean of 13.3 ± 2.3 μm (n=13 cells). The range of the middle 75% of RBPMS cell diameters in the guinea pig retina is 13.4 to 15.6 μm. In the rabbit INL, the range of the middle 75% of the RBPMS cell diameters was 13.9 to 19.8 μm. Average RBPMS soma diameter was 15.6 ± 1.9 μm (n=18 cells) in central retina and 18.8 ± 1.9 μm (n=7 cells) in peripheral retina. In a monkey retina (UC1), RBPMS cells in the central temporal retina ranged from 10.4 to 16.2 μm in diameter with a mean of 12.4 ± 1.6 μm (n=20 cells). In the nasal, inferior retina, RBPMS cell diameter ranged from 13.3 to 27.3 μm

with a mean of 20.3 ± 4.3 μm (n=11 cells). The absolute range of RBPMS somal diameters as well as their average and median diameters is given in Tables 2 and 4.

In the mouse and rat retina, about 4.5% of the RBPMS cells in the INL measured less than 10 μm in diameter. In rabbit, guinea pig, and monkey (inferior nasal) retina, none of the RBPMS cells in the INL measured less than 10 μm in diameter. In the mouse, rat and guinea pig retina, 0.8%, 3.8%, and 0.0%, respectively of the RBPMS cells in the INL measured greater than 20 μm in diameter. In rabbit and monkey retina, 12.0% and 16.7%, respectively of the RBPMS cells in the INL measured greater than 20 μm in diameter. Overall, average RBPMS somal diameter and area for mouse, rat, rabbit and monkey are similar in size to dRGCs identified using other labeling techniques (Bunt et al., 1975; Bunt and Minckler, 1977; Robson and Holländer, 1984; Buhl and Dann, 1988; Pang and Wu, 2011). The size of dRGCs in guinea pig retina has not been previously reported to our knowledge.

Somal distribution—RBPMS cells were present in all regions of the mouse, rat, guinea pig and rabbit INL, although their distribution varied, usually with a greater number of RBPMS cells in peripheral retinal regions compared to central regions. RBPMS cells were present in all regions (central temporal and nasal inferior) of the monkey retina sampled in this study.

In the mouse retina, most RBPMS somata were in mid-peripheral, and peripheral ventral and dorsal retina. In contrast, in the rat retina most RBPMS cells were in mid-peripheral and peripheral regions of the dorsal retina. In rabbit retina, a few RBPMS cells were distributed to the central retina, including the visual streak, and the majority of RBPMS somata were in peripheral and far peripheral ventral and dorsal retina. In contrast to this general pattern, in the guinea pig retina, a greater number of immunostained RBPMS cells were in central retina compared to peripheral retina. In the monkey retina (UC1), RBPMS cells in the INL were also in central temporal and nasal inferior retinal regions, although the sampling was to sparse to assess their relative distribution and number in the INL.

Identification of RBPMS cells

The somal size and distribution of RBPMS cells in both the GCL and INL strongly suggest they are RGCs. To test this idea, mouse and rat retina were double immunostained with antibodies to RBPMS, and to syntaxin 1 (HPC-1), GABA or glycine, which are established amacrine cell markers (Barnstable et al., 1985; Wässle and Boycott, 1991; Pérez de Sevilla Müller et al., 2007).

Identification of RBPMS cells in the GCL and INL—RBPMS-immunoreactive cells in the GCL did not express syntaxin 1 immunoreactivity, a marker of displaced amacrine cells in the mouse (Figure 9 AC) and rat retina. Furthermore, the majority of the RBPMS-immunoreactive cells in the GCL did not contain GABA immunoreactivity, although ~5% of the RBPMS cells contained low levels of GABA immunoreactivity (see below; Figure 10), consistent with recent reports of low levels of GABA immunoreactivity in some ganglion cells (Caruso et al., 1989; Pang and Wu, 2011; Pang et al., 2013). Furthermore, RBPMS-containing cells in the INL did not contain syntaxin 1, GABA or glycine immunoreactivity in the mouse (Figure 9 D–F) and rat retina. Together, these findings support the idea that RBPMS expression is confined to the RGC population.

Some RBPMS cells in the GCL contain low levels of GABA immunoreactivity —A small percent of the RBPMS cells in the GCL had weak GABA immunoreactivity. In the mouse retina, 6.04% ± 1.3% (75 cells/1241 cells; N=6 retinas from 3 mice) of the RBPMS-expressing cells in the GCL contained low levels of GABA immunoreactivity

(Figure 10 A–C). Their average somal diameter was 12.8 ± 2.2 μm (n=75 cells). In the rat retina, 5.3%± 1.4% (84/1571 cells; N=3 retinas from 3 rats) of the RBPMS-expressing cells in the GCL also contained low levels of GABA immunoreactivity (Figure 10 D–F). The average somal diameter of the cells co-expressing RBPMS and GABA immunoreactivity was 18.6 ± 3.1 μm (n=84 cells). In addition, in rat retina RBPMS-expressing somata contained GABA immunoreactivity was not observed 21 days after optic nerve transection (see below). These findings support the suggestion that the RBPMS cells with low levels of GABA immunoreactivity are RGCs.

The colocalization of RBPMS with GABA immunoreactivity was not evaluated in guinea pig, rabbit and monkey retina.

To test the possibility that the weak GABA immunostaining in RBPMS cells was a result of the exchange of GABA between amacrine and ganglion cells coupled by connexin 36 (Cx36), we evaluated whole-mounted retinas from a $Cx36^{-/-}$ mouse line (Deans et al., 2002). In $Cx36^{-/-}$ retinas, 0.22 ± 0.04% (10/4527 cells; N=3 retinas from 3 mice) of the RBPMS-expressing cells contained low levels of GABA immunoreactivity (Figure 11). The average size of the remaining double-immunostained cells was 10.89 ± 0.51 μm (n=22 cells). The very low number of RBPMS somata in the $Cx36^{-/-}$ retinas compared to wild-type C57BL/6J mouse retinas is consistent with the idea that there is exchange of GABA immunoreactivity between RBPMS and GABA-containing amacrine cells via Cx36 gap junctions (Pérez de Sevilla Müller et al., 2007; Völgyi et al., 2009; Pan et al., 2010).

RBPMS cells in the mouse, rat, guinea pig, rabbit and monkey GCL

The cellular expression of RBPMS was further characterized in the GCL of whole-mounted mouse, rat, guinea pig, rabbit and monkey retinas. Whole-mounted retinas were immunostained with RBPMS antibodies and counterstained with one or more of the following cellular markers, DAPI, DRAQ5, NeuroTrace or NeuN. DAPI and DRAQ5 primarily label the nucleus of RGCs, displaced amacrine cells, astrocytes and endothelial cells. NeuroTrace and NeuN are cellular markers that label the cytoplasm and nucleus, and primarily stain RGCs and displaced amacrine cells.

In the mouse retina, all RBPMS immunostained cells in the GCL were counterstained with DAPI, DRAQ5 or NeuroTrace (Figure 12). The diameter of the double labeled cells ranged from 8.1 to 29.1 μm (n=500) in the DAPI, 10.0 to 28.0 μm (n=370) in the DRAQ5, and 7.4 to 32.4 μm (n=375) in the NeuroTrace counterstained whole-mounted retinas. The range of the somal diameters of the double labeled cells was similar to the range of somal diameters of RBPMS-immunoreactive cells measured in other mouse retinas (Table 3). There was a greater number of DAPI and DRAQ5 stained nuclei that were not localized to RBPMS immunoreactive cells. In addition, there was a greater number of small diameter NeuroTrace stained cells that did not express RBPMS, and they measured from 4.4 to 14.9 μm (n=646) in diameter with an average of 9.4 ± 1.6 μm consistent with their identity as displaced amacrine cells (Perry, 1981; Pérez de Sevilla Müller et al., 2007). In the counterstained whole-mounted retinas, 49.3% (n=1039/2109) of the DAPI-, 45.4% (n=805/1775) of the DRAQ5- and of the 42.8% of the (n=441/1031) NeuroTrace-stained cells contained RBPMS immunoreactivity. The percentage of RBPMS immunoreactive cells in these preparations is similar to other estimates of the percent of RGCs in the GCL of the mouse retina (Jeon et al., 1998; Pang and Wu, 2011).

In the rat retina (Figure 13), as well as the guinea pig and rabbit retina, there was a similar pattern of labeling in the GCL. RBPMS was mainly expressed by medium and large somata. There were more numerous DAPI and DRAQ5 stained nuclei, and small diameter somata

labeled by NeuroTrace or NeuN antibodies, which did have RBPMS immunoreactivity (data not shown).

In segments of whole-mounted dorsal nasal monkey retina (UC1), all RBPMS immunostained cells in the GCL were counterstained with DRAQ5 or NeuN immunoreactivity (Figure 14). Double labeled cells ranged in diameter from 10.6 to 27.1 μm (n=203) in the DRAQ5 and 11.0 to 29.6 μm (n=231) in the in the NeuN counterstained retinas, consistent with earlier reports of the somal size of RGCs in the monkey retina (Table 3). NeuN cells lacking RBPMS immunoreactivity measured from 6.6 to 17.7 μm (n=338) in diameter with a mean of 11.1 ± 2.1 μm consistent with their identity as displaced amacrine cells (Koontz et al., 1993). There was an overlap of the somal diameters of the smallest RBPMS and the largest NeuN immunoreactive cells (Figure 14 F).

Overall, there was a greater number of DRAQ5 stained nuclei than NeuN immunoreactive somata at the same retinal eccentricity (Figure 14 B, E). Furthermore, there was a greater number of DRAQ5 stained nuclei then the small and often faintly immunostained NeuN cells, which lacked RBPMS (Figure 14 C, F). These findings suggest that NeuN is not detectable in many of the displaced amacrine cells in the monkey GCL.

RBPMS cell loss after optic nerve crush or transection

In the mouse retina (N=4), 21 days after unilateral optic nerve crush, the number of RBPMS-expressing somata in the GCL of the injured retina was markedly reduced (86.0 ± 0.1%) compared to the number of RBPMS cells in the GCL of the non-injured, contralateral retina (Figure 15). The number of immunostained cell bodies in the GCL was reduced in all retinal quadrants and at all eccentricities. RBPMS-containing cell bodies remaining in the GCL of the retinas with the crushed optic nerve ranged from 11.1 to 35.1 μm (n=2092) in diameter with a mean of 15.8 ± 3.3 μm. Their immunostaining levels varied from weak to strong, compared with the more uniformly immunostained RBPMS cells in the GCL of non-injured retinas.

In the rat retina (N=3), the number of RBPMS-expressing somata in the GCL 21 days after unilateral optic nerve transection was reduced by 98.2 ± 0.1% compared to the number of RBPMS cells in the non-axotomized (contralateral) retina (Figure 16). Immunoreactive cell bodies in the GCL were lost in all retinal quadrants and at all eccentricities. RBPMS-containing cells in the GCL of the axotomized retina displayed a range of immunostaining levels, from weak to strong, compared with RBPMS immunostaining in the GCL of the contralateral, non-injured retinas. Consistent with these findings was the marked reduction of the level of RBPMS immunoreactivity on Western blots of retinal extracts collected 21 days after unilateral optic nerve transection (Figure 1, lanes 7 and 10).

Specific and weak RBPMS immunoreactivity was also in some endothelial cells, which form blood vessels in the GCL and nerve fiber layer (NFL) of optic nerve transected rat retinas (Figure 16 E). RBPMS immunostaining was absent in the GCL of optic nerve transected retinas incubated in the primary antibody with the RBPMS polypeptide used for generating the RBPMS antibodies (Figure 16 F). Immunostaining was absent in retinas incubated with secondary antibody alone, indicating that the very, weak RBPMS immunostaining was not due to a non-specific immune reaction between the retinal cells and the secondary antibody.

Co-expression of RBPMS and RGC markers in the mouse and rat retina

RBPMS-containing cells in the GCL of the mouse and rat retina were characterized using antibodies to Brn3a, SMI-32 and melanopsin, established RGC markers (Xiang et al., 1995; Hattar et al., 2002; Coombs et al., 2006). Brn3a, a POU-domain containing transcription

factor, is often used as a specific marker of RGCs (Xiang et al., 1995; Nadal-Nicolás et al., 2009; Galindo-Romero et al., 2011). SMI-32, is directed to neurofilament H, and the SMI-32 antibody immunostains medium and large RGCs (Coombs et al., 2006). Melanopsin is an opsin protein expressed in medium and large RGCs. The melanopsin antibody we used to immunostain mouse retina labels M1 – 3 ipRGCs, and the melanopsin antibody used to immunostain rat retina labels M1 ipRGCs (Hattar et al., 2002; Coombs et al., 2006; Baver et al., 2008; Berson et al., 2010; Pérez de Sevilla Müller et al., 2010b).

In the mouse retina (N=4) all (n=2615 cells) of the Brn3a immunoreactive somata contained RBPMS. Conversely most (81.6 ± 0.7%) of the RBPMS somata contained Brn3a immunoreactivity (Figure 17 A–C). RBPMS cells lacking Brn3a immunoreactivity averaged 16.9 ± 2.6 μm (n=455 cells) in diameter, and were similar in size to the RBPMS-immunoreactive cells (Table 2) measured in other mouse retinas. Triple label immunostaining studies with RBPMS, Brn3a and GABA antibodies, revealed the same percentage (79%) of RBPMS cells expressed Brn3a immunoreactivity, and in addition, some weak GABA immunoreactive cells expressed both RBPMS and Brn3a immunoreactivity (data not shown). There were no examples of RBPMS- and GABA-containing cells that lacked Brn3a immunoreactivity. In the rat retina (N=4), all (n=1771 cells) of the Brn3a immunoreactive somata also contained RBPMS immunoreactivity, and most (78.9 ± 5.0%) of the RBPMS-immunoreactive somata contained Brn3a (Figure 17 D–F). RBPMS cells lacking Brn3a immunoreactivity averaged 13.8 μm (n=46 cells) in diameter, and were in the bottom half of the range of RBPMS-immunoreactive cells (Table 2) measured in other rat retinas.

In the mouse retina (N=3), all of the SMI-32- (n=97) and melanopsin- (n=32 cells) expressing RGCs had RBPMS immunoreactivity (data not shown). In rat retina (N=1), all SMI-32- (n=129) and melanopsin- (n=61) containing RGCs also had RBPMS immunoreactivity (Figure 18). The RBPMS cells expressing SMI-32 measured from 11.4 to 36.8 μm in diameter and the melanopsin measured from 13.8 to 20.2 μm in diameter in mouse and rat retina, consistent with earlier estimates of the somal size of these RGCs in mouse retina (Hattar et al., 2002; Coombs et al., 2006; Berson et al., 2010).

In the Thy1-CFP transgenic mouse retina (N=6), where CFP fluorescence is expressed in RGCs driven by the Thy1 promoter (Feng et al., 2000), small, medium and large RBPMS somata with CFP fluorescence were distributed to the GCL in all retinal regions (Figure 19). These cells ranged from 9.3 to 29.7 μm (n=90 cells) in diameter. In the GCL, 82.3 ± 2.6% (900/1094 cells) of the RBPMS cells contained CFP fluorescence, and conversely, 84.2 ± 3.1% of the CFP-fluorescent cells contained RBPMS based on counts averaged from all of the retinal regions.

Discussion

RBPMS, a member of the RRM family of RNA-binding proteins, is strongly and exclusively expressed in RGCs and dRGCs in mouse, rat, guinea pig, rabbit and monkey retina. These studies extend earlier findings that RBPMS and RBPMS2 mRNAs are localized to the GCL in the mouse retina at embryonic day 14.5 (Diez-Roux et al., 2011). RBPMS immunoreactivity and RBPMS2 mRNAs are also reported in adult rat RGCs (Piri et al., 2006; Kwong et al., 2010). More recently, Hermes/RBPMS immunoreactivity was reported to be expressed in embryonic *Xenopus* and zebrafish RGCs and their axons (Gerber et al., 1999; Hörnberg et al., 2013) indicating its conserved expression in both non-mammalian and mammalian retinas.

Overall, in all of the mammalian species evaluated in this study, RBPMS immunoreactivity was mainly localized to medium and large cells in the GCL, which range from ~10 to 30 μm in diameter (Figures 4 and 5; Table 2), and their somal position, size, distribution, density and percentage occurrence in the GCL are similar to earlier descriptions of RGCs. In contrast, displaced amacrine cells, which are also in the GCL do not express RBPMS. These findings are consistent with the expression of RBPMS immunoreactivity in rat RGCs identified by retrograde labeling following Fluorogold application to the transected optic nerve stump (Kwong et al., 2010; Kwong et al., 2011) and their loss in the mouse and rat retina following optic nerve crush or transection, as shown by both the Western blot and immunohistochemical studies.

RBPMS immunoreactivity is also expressed in medium, and some small and large cell bodies located in the INL at the border of the IPL, consistent with their identity as dRGCs in all of the mammalian species evaluated in this study (Figure 8 and Table 2). Cell bodies containing RBPMS immunoreactivity are as a group larger than adjacent amacrine cell bodies in the INL, and in mouse and rat retina they do not contain syntaxin 1, GABA or glycine immunoreactivity, which are expressed by amacrine cells (Barnstable et al., 1985; Wässle and Boycott, 1991). Furthermore, they are not Neurod6-containing amacrine cells reported in the mouse retina, which measure less than 10 μm in diameter and express syntaxin 1 (HPC-1), but not GABA or glycine immunoreactivity (Kay et al., 2011). In addition, in the rat retina, most RBPMS cells in the INL are lost three weeks after optic nerve transection.

RBPMS somal size in the GCL compared to RGCs—The average RBPMS somal diameters in the mouse, rat, guinea pig, rabbit and monkey GCL range from 12.7 to 17.9 μm (Table 2).

In mouse and rat retina, RBPMS somal diameters range from ~9 to 35 μm and they are similar in size to some of the small, and all of the medium and large Nissl stained cell bodies in the GCL, which are now recognized as RGCs in the mouse (Dräger and Olsen, 1981) and rat retina (Fukuda, 1977; Perry, 1981). Furthermore, somal sizes of RBPMS and RGC somata retrogradely labeled by HRP, Neurobiotin or the fluorescent dyes, Lucifer yellow and DiI are similar in the majority of studies of mouse and rat retina (Bunt et al., 1974; Dräger and Olsen, 1980; 1981; Perry, 1981; Linden, 1987; Doi et al., 1995; Huxlin and Goodchild, 1997; Sun et al., 2002a; b; Pang and Wu, 2011) (Table 3). RBPMS somata and RGCs measuring less than 9 μm in diameter occur more commonly in mouse retina than rat retina. In mouse retina, there is a relatively greater number of Nissl stained RGCs smaller than 9 μm in diameter (Dräger and Olsen, 1981) than the number of RBPMS somata smaller than 9 μm in diameter (less than 1% in the present study). The higher frequency of small Nissl stained RGCs in mouse retina can be accounted for by shrinkage from tissue processing (Fukuda, 1977; Dräger and Olsen, 1981). Finally, RBPMS somata in the mouse and rat retina are larger as a group in peripheral retina compared to central retina (Figures 6 and 7), consistent with reports that larger RGCs are distributed to peripheral retinal regions (Bunt et al., 1974; Dräger and Olsen, 1980; 1981; Pang and Wu, 2011).

In the guinea pig and rabbit GCL, RBPMS somal diameters average 16.9 μm and 15.5 μm, respectively. These measurements were made from multiple retinal regions of two guinea pig and two rabbit retinas (Table 2). The average size of mouse, rat and guinea pig RBPMS somata are slightly larger than rabbit RBPMS somata. Similar to mouse and rat retina, the range of RBPMS somal diameters in guinea pig is likely to be similar to the range of somal diameters of RGCs retrogradely labeled by HRP, which are reported to be <10 to >20 μm in diameter (Do-Nascimento et al., 1991). There is also a similar distribution of the range of RBPMS somal diameters in the rabbit retina; medium to large Nissl stained cell bodies

measured about 10 to 25 μm (Vaney, 1980; Oyster et al., 1981) and RGCs retrogradely labeled by HRP measured 10 to 33 μm (Robson and Holländer, 1984) (Table 3).

In the central temporal monkey retinal sample, RBPMS somal diameters ranged from 6.5 to 25.4 μm with an average of 12.7 ± 2.5 μm (Table 2). RBPMS somal diameters in the inferior nasal retinal sample were larger and ranged from 10 to 38 μm with an average of 16.8 ± 3.8 μm (Table 2). The range of RBPMS somal diameters are similar to RGC somal diameters that project to the lateral geniculate nucleus and superior colliculus. RGC somas ranged from 8–10 μm in diameter in the central retina that included the fovea and parafovea, and 11 to >20 μm in diameter in peripheral retinal regions (Bunt et al., 1975; Perry and Cowey, 1984; Perry et al., 1984b) (Table 3).

RBPMS somal distribution in the GCL compared to RGCs—RBPMS cells were distributed to all retinal regions with a gradient of immunoreactive cells from central to peripheral in the mouse, rat and guinea pig retina. In rabbit retina, the highest number of RBPMS somata is in the visual streak. These observations are consistent with the distribution of RGCs in these species (Fukuda, 1977; Dräger and Olsen, 1980; Vaney, 1980; Dräger and Olsen, 1981; Oyster et al., 1981; Perry, 1981; Perry and Cowey, 1985; Wässle et al., 1990; Do-Nascimento et al., 1991; Salinas-Navarro et al., 2009; Pang and Wu, 2011).

There is a good match of the distribution of RBPMS cell density in mouse retina with estimates of RGC density based on HRP retrograde labeling, ranging from ~5000 cells/mm^2 in central retina to 1500 cells/mm^2 in peripheral retina (Dräger and Olsen, 1980). Estimates of overall RBPMS cell density are likely to be closer to more recent estimates of RGC density based on dye- and retrograde cell labeling, which range from 2944 to 3817 cells/mm^2 (Galindo-Romero et al., 2011; Pang and Wu, 2011) than estimates of RGC density based on NeuN immunostaining, which range from ~4600 to 5012 cells/mm^2 (Buckingham et al., 2008; Templeton et al., 2009). This is because estimates of RGC density based on NeuN immunostaining are biased by the expression of NeuN immunoreactivity in displaced amacrine cells (Buckingham et al., 2008). There is variability in the number of RGCs in different mouse strains and the C57BL/6 strain from Jackson Laboratory is estimated to have ~54,600 (± 3910) total ganglion cells based on counts of optic nerve axons (Williams et al., 1996). The area of a C57BL/6J mouse retina is 15.66 mm^2 (Remtulla and Hallett, 1985) and therefore the overall RGC density is expected to be about 3487 cells/mm^2. The density of RBPMS-containing cells in mouse retina is likely to be close to this estimate.

In rat retina, RBPMS cell density in central retina at 1 mm from the optic nerve head was 2938 ± 569 cells/mm^2. This estimate is close to an earlier estimate in rat retina of RBPMS somal density (2744 cells/mm^2) at 1 mm from the optic nerve head (Kwong et al., 2011). These cell density estimates are lower than previous estimates of RGC density based on Nissl stained cell bodies in central mouse (Dräger and Olsen, 1981) and rat (Fukuda, 1977) retina, which undoubtedly included displaced amacrine cells in the cell counts. Estimates of RBPMS cell density in rat retina is likely to be similar to earlier estimates of RGC density based on retrograde labeling ranging from 3000 cells/mm^2 in central retina to 1600 cells/mm^2 in peripheral retina (Perry, 1981; Linden and Perry, 1982), and overall RGC density from 2144 to 3817 cells/mm^2 (Villegas-Perez et al., 1993; Berkelaar et al., 1994).

The distribution and overall RBPMS cell density was not determined in guinea pig, rabbit and monkey retina because of the small number of retinas sampled in this study. However, comparison of the average RBPMS cell densities from the limited number of guinea pig, rabbit and monkey retinal fields sampled show a good correspondence to published average RGC densities found by other methods (Vaney, 1980; Oyster et al., 1981; Wässle et al., 1990; Do-Nascimento et al., 1991).

RBPMS somal size in the INL compared to dRGCs—Average RBPMS somal diameters in the INL of the mouse, rat, guinea pig, rabbit and monkey retina range from 12.4 to 20.3 μm (Table 2).

In the mouse and rat INL, there is good agreement of the somal sizes of RBPMS somata that range from ~8 to 20 μm in diameter and RGC somata identified by retrograde labeling by HRP or Neurobiotin that range from 7 to 19 μm (Dräger and Olsen, 1980; Perry, 1981; Linden, 1987; Buhl and Dann, 1988; Pang and Wu, 2011) (Table 4). Guinea pig and rabbit retinas also have medium and large diameter RBPMS somata in the INL that average 13.3 μm and 16.5 μm in diameter, respectively (Table 2). As in the mouse and rat retina, in the rabbit retina, there is good agreement of the size of RBPMS somata, which range from ~8 to 20 μm in diameter and RGC somata identified by retrograde labeling by HRP (Robson and Holländer, 1984) (Table 4). In the monkey INL, RBPMS somal diameters ranged from 13.3 to 27.3 μm with an average of 20.3 ± 4.3 μm (Table 2). The average size of RBPMS cells is larger in monkey retina compared to mouse, rat, guinea pig and rabbit retina. RBPMS cells are similar in size compared to dRGCs identified by HRP retrograde labeling from the lateral geniculate nucleus of the *Macaca fascicularis* and *Macaca mulatta* (Bunt et al., 1975; Bunt and Minckler, 1977) (Table 4).

RBPMS somal distribution in the INL compared to dRGCs—A sparse number of RBPMS somata were distributed to the INL in all retinal regions of the mouse, rat, guinea pig and rabbit retina. These findings are consistent with earlier estimates of a low percentage of dRGCs in mouse and rat retina (Dräger and Olsen, 1981; Perry, 1981; Robson and Holländer, 1984; Liu and Jen, 1986; Linden, 1987; Do-Nascimento et al., 1991; Pang and Wu, 2011). The distribution of RBPMS somata in mouse and rat retina match the majority of studies, which report that dRGCs identified by retrograde transport of HRP or fluorescent dyes are distributed to all retinal regions with their greatest number in mid-peripheral, peripheral and temporal retina (Dräger and Olsen, 1980; 1981; Liu and Jen, 1986; Linden, 1987; Buhl and Dann, 1988; Pang and Wu, 2011). In the guinea pig retina, there is also a gradient of RBPMS cells from central to peripheral retina with a greater number of cells in the central retina. In rabbit retina, there are a few RBPMS somata in and near the visual streak consistent with a report of a very low number (0.1%) of dRGCs in the visual streak and a higher number (5%) of dRGCs in peripheral retina (Robson and Holländer, 1984).

GABA expression in RBPMS immunoreactive cells in the GCL

Weak GABA immunostaining in some RGCs has been noted in several mammalian species, including the mouse and monkey retina (Wässle et al., 1990; Koontz et al., 1993; Pang and Wu, 2011; Pang et al., 2013). About 5% of the RBPMS cells in the mouse and rat GCL expressed a low level of GABA immunoreactivity. In mouse and rat retina, these cells averaged 12.4 μm and 18.6 μm in diameter, respectively and are larger as a group than most displaced amacrine cells, which measure between 7 and 12 μm in diameter (Perry, 1981; Pérez de Sevilla Müller et al., 2007). These findings are congruent with an earlier report based on the retrograde labeling of RGCs from the superior colliculus, of a low percent (~6%) of GABA-containing RGCs that range from 10 to 12 μm in diameter in the rat retina (Caruso et al., 1989). In addition, there is a loss of RBPMS cells containing GABA immunoreactivity after optic nerve transection. Together, these findings support the identity of RBPMS cells expressing GABA in the mouse and rat retina as RGCs.

Earlier studies have demonstrated that Cx36 gap junctions form the majority of heterologous coupling between amacrine and ganglion cells (Pan et al., 2010), and our experiments showed very few (0.2%) weak GABA immunostained RBPMS cells in the Cx36 null line. Our observations therefore suggest GABA immunoreactivity in RBPMS cell bodies

originates from GABA-containing amacrine cells that are mainly coupled by Cx36 to RBPMS cells. Consistent with this idea is the dye coupling of RGCs with ~4% of the GABA-containing amacrine cells and ~10% of the displaced amacrine cells in the mouse retina (Pang et al., 2013). A precedent for amino acid exchange between retinal neurons is the labeling of cone bipolar cells by glycine via gap junctions with AII amacrine cells (Cohen and Sterling, 1986; Vaney et al., 1998; Deans et al., 2002). The remaining RBPMS-expressing cells with GABA immunoreactivity may be coupled by different connexins that are expressed in ganglion cells. For instance, Cx45 is expressed by bistratified ganglion and amacrine cells, and Cx30.2 by multiple ganglion cell types, as well as with amacrine cells (Schubert et al., 2005; Pan et al., 2010; Pérez de Sevilla Müller et al., 2010a).

RBPMS expression compared to other cellular markers of displaced amacrine and ganglion cells in the GCL

The expression of RBPMS was evaluated with the cellular makers, DAPI, DRAQ5, NeuroTrace and NeuN, which were used to identify RGCs and displaced amacrine cells in the GCL.

In whole-mounted mouse, rat, guinea pig, rabbit and monkey retinas, all RBPMS-containing cells were stained by DAPI, DRAQ5 or NeuroTrace or immunostained with NeuN antibodies. The somal diameters of the RBPMS cells in the mouse and monkey preparations have the same range as RBPMS cells measured in other mouse and monkey retinas (Table 3), consistent with their identity as RGCs. Furthermore, the percentage of RBPMS-expressing cells in the GCL of whole-mounted mouse retinas, is similar to other estimates of the percentage of RGCs in the mouse GCL (Jeon et al., 1998; Pang and Wu, 2011). The majority of NeuroTrace stained cells in these preparations have small somal diameters, and in mouse, rat, guinea pig and rabbit retinas these cells are in the size range that was previously reported for displaced amacrine cells (Perry, 1981; Do-Nascimento et al., 1991; Koontz et al., 1993; Pérez de Sevilla Müller et al., 2007). Together, these findings are consistent with the exclusive localization of RBPMS to RGCs.

Finally, there is an overlap of the somal diameters of the smallest RBPMS cells and the largest NeuN immunoreactive cells, which do not contain RBPMS immunoreactivity in the whole-mounted monkey retinal samples. These non-RBPMS, NeuN immunoreactive cells may be large displaced amacrine cells or alternatively, small RGCs that do not express RBPMS. This later possibility is not likely in our view, based on the localization of RBPMS immunoreactivity to RGCs and not to displaced amacrine cells in the other species we have evaluated in this study.

RBPMS loss after optic nerve transection or crush

In the mouse and rat retina, 3 weeks after optic nerve injury, the number of RBPMS-expressing cells in the GCL of the injured retina is markedly reduced in agreement with earlier observations using another RBPMS antibody (Kwong et al., 2011). These findings are also consistent with the reduction of RBPMS immunoreactivity on Western blots of rat retina after optic nerve transection. The range of the RBPMS somal diameters in the nerve crushed mouse retina was similar to the range of somal diameters in the contralateral, non-operated retina (Table 2), suggesting the injury affected all RGC types. Furthermore, the remaining RBPMS-containing cells in the GCL of the injured retina varied in immunostaining from very low to high levels suggesting RBPMS levels are influenced by nerve injury. In rat retina, the remaining RBPMS-containing cells also have other established RGC markers, including intermediate neurofilament and melanopsin immunoreactivity congruent with their identity as RGCs. Together these findings also support the idea that RGCs express RBPMS immunoreactivity. In addition, retrograde

transport studies report that greater than 99% of the labeled RGCs express RBPMS immunoreactivity in the rat retina (Kwong et al., 2010; Kwong et al., 2011), also supporting the identity of RBPMS immunoreactive cells as RGCs.

A very, low level of specific RBPMS immunoreactivity was also observed in endothelial cells in the GCL and NFL after optic nerve injury in the mouse and rat retina. These findings suggest an injury response with an increase of RBPMS activity in retinal vessels, concomitant with numerous other patho-physiological changes that occur following RGC axonal injury, including activation of microglia and caspases, and altered regulation of cytokines, chemokines and free radicals (Cui et al., 2009; Fischer and Leibinger, 2012).

RBPMS expression compared to other RGC markers

The expression of RBPMS was evaluated with three commonly employed markers for RGCs, Brn3a, SMI-32 and melanopsin. Brn3a is expressed by numerous RGCs in mouse, rat, cat and monkey retina (Xiang et al., 1995; Nadal-Nicolás et al., 2009; Galindo-Romero et al., 2011). Brn3a is reported to be in about 85% and 95% of the RGCs of mouse and rat retina, respectively (Nadal-Nicolás et al., 2009; Galindo-Romero et al., 2011; Nadal-Nicolás et al., 2012). In contrast, SMI-32 and melanopsin are in a smaller percentage of RGCs. SMI-32 is expressed by multiple RGC types having a medium or large somal diameter, and small, medium and large dendritic fields (Coombs et al., 2006). Melanopsin is in multiple RGC types having a medium somal diameter and large and sparse dendrites, and these cells constitute 1–3% of the RGCs in the mouse and rat retina (Hattar et al., 2002; Baver et al., 2008; Berson et al., 2010; Galindo-Romero et al., 2013).

RBPMS is expressed in all Brn3a, SMI-32 and melanopsin immunoreactive cells, consistent with the expression of RBPMS by all RGCs. There is about 20% more RBPMS-immunoreactive somata then Brn3a somata in mouse and rat retina. Other studies also suggest that Brn3a is expressed by a large percentage, but not all RGCs. For example, a greater number of RGCs are retrogradely labeled by fluorescent dyes than express Brn3a in both the mouse and rat retina (Nadal-Nicolás et al., 2009; Galindo-Romero et al., 2011; Nadal-Nicolás et al., 2012). Furthermore, most ipRGCs do not express Brn3a, and RGCs expressing Brn3a do not project to the suprachiasmatic nucleus of the hypothalamus, accessory optic system and pretectal nuclei (Quina et al., 2005; Jain et al., 2012; Nadal-Nicolás et al., 2012). Finally, there are a greater number of RBPMS cells than strongly fluorescent CFP-containing cells that are likely to be RGCs in the Thy1-CFP transgenic mouse retina (Feng et al., 2000; Raymond et al., 2008) consistent with the partial labeling of the RGC population by CFP in this line. Together, these findings indicate that RBPMS is likely to be expressed in the entire RGC population, including the dRGCs.

Guinea pig, rabbit and monkey retinas were not evaluated for the co-expression of RBPMS and these markers for RGCs; although, based on the number of RBPMS cells in these species, it seems highly likely that there would be co-expression of RBPMS and commonly used RGC markers.

RBPMS expression in RGCs

RBPMS immunoreactivity is mainly confined to the cytoplasm of the soma, although it is also present in proximal dendrites and finer caliber dendrites in the IPL. RBPMS immunoreactivity in the somata is consistent with a role in posttranscriptional regulation of gene expression, since proteins with the RRM motif participate in mRNA translation, processing, transport and stability (Burd and Dreyfuss, 1994; Shimamoto et al., 1996; Maris et al., 2005; Lunde et al., 2007). RBPMS also has a role in transcriptional regulation of gene expression; RBPMS interaction with the Smad proteins is enhanced in a TGF-β dependent

manner, and promotes Smad4 translocation to the nucleus to mediate transcriptional activity of TGF-β responsive genes (Sun et al., 2006). The function of RBPMS in ganglion cells and the retina are unknown, although RBPMS interaction with Smad4 to influence TGF-β signaling suggests a role in retinal development and growth (Duenker, 2005; Wordinger and Clark, 2007). Consistent with this idea are findings that in mouse retina, a conditional *Smad4* deletion results in alterations of RGC development and defects in the targeting of RGC axons to the optic nerve head (Murali et al., 2011). RBPMS2 mRNA (Gerber et al., 1999) and Hermes/RBPMS immunoreactivity (Hörnberg et al., 2013) is expressed exclusively in RGCs including their axons and axonal terminals in embryonic *Xenopus* and zebrafish retina. Interestingly, lost of function studies targeting *Xenopus hermes 1* and *2*, and zebrafish *rbpms2a* and *2b*, reveals a reduction of axonal terminal complexity as well as an increase in the presynaptic density of optic axon terminals (Hörnberg et al., 2013). In contrast, RBPMS immunoreactivity is mainly confined to the soma of adult mammalian RGCs. Perhaps these differences in the RBPMS expression patterns are due to down regulation of RBPMS in mammalian RGC axons after axonal and synapse formation or the selectively localized of RBPMS2 to RGC axons and terminals in the mammalian retina.

RBPMS and RBPMS2, in addition to other transcription factors are proving to be excellent markers for RGCs in both mammalian and non-mammalian species. For instance, the POU-domain containing transcription factor proteins Brn3a (*Pou4f1*), Brn3b (*Pou4f2*) and Brn3c (*Pou4f3*) are exclusively expressed by RGCs in the mouse, rat and monkey retina, although they are not expressed in the entire RGC population (Xiang et al., 1995; Quina et al., 2005; Galindo-Romero et al., 2011; Nadal-Nicolás et al., 2012). Isl1 and Isl2, LIM homeodomain-containing transcription factors, are expressed by chicken and mouse RGCs, as well as by bipolar and amacrine cells (Galli-Resta et al., 1997; Edqvist et al., 2006; Elshatory et al., 2007). In addition, Math5, a bHLH factor specifies RGCs early in embryogenesis (Brown et al., 2001; Wang et al., 2001). Other transcription factors, including Tbx5, Smad2 and 5330410G16Rik may also be exclusively expressed in RGCs based on their strong presence in the GCL of the embryonic mouse retina (Diez-Roux et al., 2011).

RBPMS is superior to other markers that identify RGCs, including extracellular, calcium binding, cytoskeletal, and nuclear proteins as well as neuroactive peptides. Commonly used markers for ganglion cells, include Thy1 (Barnstable and Dräger, 1984), calretinin, calbindin and parvalbumin (Pasteels et al., 1990; Sanna et al., 1990; Kim and Jeon, 2006; Lee et al., 2010), neurofilaments (Dräger and Hofbauer, 1984; Kong and Cho, 1999; Coombs et al., 2006), NeuN (Buckingham et al., 2008; Templeton et al., 2009; Johansson et al., 2010) and substance P (Brecha et al., 1987). Most of these RGC markers are not expressed in all RGCs and often they are localized to other retinal cell types (Perry et al., 1984a; Brecha et al., 1987; Pasteels et al., 1990; Sanna et al., 1990; Peichl and González-Soriano, 1993; Kong and Cho, 1999; Buckingham et al., 2008; Raymond et al., 2008; Johansson et al., 2010; Kwong et al., 2011). In contrast, RBPMS is distributed to the entire cell body and it is only localized to RGCs and dRGCs.

RBPMS expression in other mammalian and non-mammalian retinas

The robust and consistent expression of RBPMS by RGCs and dRGCs in the five mammalian species we studied supports the suggestion that this RNA-binding protein would also be expressed by RGCs of other mammalian species. Of interest would be to determine if RBPMS is expressed by all or a subgroup of RGCs in other mammalian species, and if there is a differential expression of RBPMS and RBPMS2, since the *RBPMS2* gene is also expressed in mouse and rat RGCs (Piri et al., 2006; Diez-Roux et al., 2011). RBPMS2 is also expressed in the GCL of embryonic *Xenopus* and zebrafish retina (Hörnberg et al., 2013), but not in the chick retina (Wilmore et al., 2005). The failure to detect RBPMS2/

Hermes in chick retina could be due to the presence of other alternatively spliced RBPMS forms that were not detected by the *in situ* hybridization probes.

It would be of interest to further delineate the expression patterns of both RBPMS and RBPMS2 in other non-mammalian and mammalian species to better understand the evolution of this family of RNA-binding proteins. These findings may also provide further insights into their functional role in the retina (Hörnberg and Holt, 2013) and elsewhere in the nervous system.

RBPMS as a RGC marker

Identification of RGCs and the entire RGC population is advantageous for a variety of experimental studies (Kwong et al., 2011; Sargoy et al., 2013). For instance, neurodegeneration and neuroprotection studies often use the visual system as a model for CNS injury, and RGC number and density are often quantified after an experimental manipulation. Having an exclusive marker for RGCs such as RBPMS that identifies the entire population of RGCs is therefore of great value. Furthermore, RBPMS antibodies are likely to be useful for evaluating RGC number in chronic disease models, including glaucoma, or in acute injury models, such as optic nerve injury or retinal ischemia (Kwong et al., 2011), and for determining the efficacy of therapeutic agents that are being tested to ameliorate or eliminate RGC degeneration.

Immunohistochemical identification of RGCs provides an excellent alternative to retrograde labeling of RGCs with several advantages, including the avoidance of experiment-induced tissue damage and a more complete and exclusive labeling of the RGC population. RBPMS antibodies could also be used as an *in vitro* tool for identifying RGCs in cell cultures. Finally, the RBPMS gene could be utilized for driving expression in RGCs in transgenic animals, or a tag for viral-mediated gene therapy.

Acknowledgments

Support: This research and development project was conducted by the authors at the David Geffen School of Medicine at UCLA and is made possible by a contract agreement that was awarded and administered by the U.S. Army Medical Research & Materiel Command (USAMRMC) and the Telemedicine & Advanced Technology Research Center (TATRC), at Fort Detrick, MD under Contract Number: W81XWH-10-2-0077. Support for these studies are also from NIH EY04067, NIDDDK P30 DK41301 (UCLA Cure Center Core) and a VA Merit Review (NCB). NCB is a VA Career Research Scientist.

We thank Drs. Arlene Hirano and Steve Barnes, and Allison Sargoy for their comments on the manuscript and their fruitful discussions of this project, Dr. Kristopher Sheets for helpful discussions and assistance in writing scripts for quantification of RBPMS cell size, number and density, and Hinekura Tehapukino for her assistance in quantification of the immunostained retinas. The connexin 36 knockout mouse retinas were developed by Dr. David L. Paul (Harvard University) and supported by NIH EY014127 and P-30 HD18655 to the IDDRC at Children's Hospital, Boston. We also thank the primate neurophysiology lab at UCLA and Drs. Teresa Puthussery and W. Rowland Taylor (Oregon Health and Science University) for providing the monkey retinas.

Literature Cited

Badea TC, Nathans J. Quantitative analysis of neuronal morphologies in the mouse retina visualized by using a genetically directed reporter. J Comp Neurol. 2004; 480:331–351. [PubMed: 15558785]

Barnstable CJ, Dräger UC. Thy-1 antigen: a ganglion cell specific marker in rodent retina. Neuroscience. 1984; 11:847–855. [PubMed: 6146113]

Barnstable CJ, Hofstein R, Akagawa K. A marker of early amacrine cell development in rat retina. Brain Res. 1985; 352:286–290. [PubMed: 3896407]

Baver SB, Pickard GE, Sollars PJ, Pickard GE. Two types of melanopsin retinal ganglion cell differentially innervate the hypothalamic suprachiasmatic nucleus and the olivary pretectal nucleus. Eur J Neurosci. 2008; 27:1763–1770. [PubMed: 18371076]

Berkelaar M, Clarke DB, Wang YC, Bray GM, Aguayo AJ. Axotomy results in delayed death and apoptosis of retinal ganglion cells in adult rats. J Neurosci. 1994; 14:4368–4374. [PubMed: 8027784]

Berson DM, Castrucci AM, Provencio I. Morphology and mosaics of melanopsin-expressing retinal ganglion cell types in mice. J Comp Neurol. 2010; 518:2405–2422. [PubMed: 20503419]

Brecha N, Johnson D, Bolz J, Sharma S, Parnavelas JG, Lieberman AR. Substance P-immunoreactive retinal ganglion cells and their central axon terminals in the rabbit. Nature. 1987; 327:155–158. [PubMed: 2437459]

Brown NL, Patel S, Brzezinski J, Glaser T. Math5 is required for retinal ganglion cell and optic nerve formation. Development. 2001; 128:2497–2508. [PubMed: 11493566]

Buckingham BP, Inman DM, Lambert W, Oglesby E, Calkins DJ, Steele MR, Vetter ML, Marsh-Armstrong N, Horner PJ. Progressive ganglion cell degeneration precedes neuronal loss in a mouse model of glaucoma. J Neurosci. 2008; 28:2735–2744. [PubMed: 18337403]

Buhl EH, Dann JF. Morphological diversity of displaced retinal ganglion cells in the rat: a lucifer yellow study. J Comp Neurol. 1988; 269:210–218. [PubMed: 3356810]

Bunt AH, Hendrickson AE, Lund JS, Lund RD, Fuchs AF. Monkey retinal ganglion cells: morphometric analysis and tracing of axonal projections, with a consideration of the peroxidase technique. J Comp Neurol. 1975; 164:265–285. [PubMed: 810500]

Bunt AH, Lund RD, Lund JS. Retrograde axonal transport of horseradish peroxidase by ganglion cells of the albino rat retina. Brain Res. 1974; 73:215–228. [PubMed: 4133900]

Bunt AH, Minckler DS. Displaced ganglion cells in the retina of the monkey. Invest Ophthalmol Vis Sci. 1977; 16:95–98. [PubMed: 401780]

Burd CG, Dreyfuss G. Conserved structures and diversity of functions of RNA-binding proteins. Science. 1994; 265:615–621. [PubMed: 8036511]

Caruso DM, Owczarzak MT, Goebel DJ, Hazlett JC, Pourcho RG. GABA-immunoreactivity in ganglion cells of the rat retina. Brain Res. 1989; 476:129–134. [PubMed: 2914207]

Cohen E, Sterling P. Accumulation of (3H)glycine by cone bipolar neurons in the cat retina. J Comp Neurol. 1986; 250:1–7. [PubMed: 3734165]

Coombs J, van der List D, Wang GY, Chalupa LM. Morphological properties of mouse retinal ganglion cells. Neuroscience. 2006; 140:123–136. [PubMed: 16626866]

Cui Q, Yin Y, Benowitz LI. The role of macrophages in optic nerve regeneration. Neuroscience. 2009; 158:1039–1048. [PubMed: 18708126]

Deans MR, Volgyi B, Goodenough DA, Bloomfield SA, Paul DL. Connexin36 is essential for transmission of rod-mediated visual signals in the mammalian retina. Neuron. 2002; 36:703–712. [PubMed: 12441058]

Dedek K, Breuninger T, de Sevilla Müller LP, Maxeiner S, Schultz K, Janssen-Bienhold U, Willecke K, Euler T, Weiler R. A novel type of interplexiform amacrine cell in the mouse retina. Eur J Neurosci. 2009; 30:217–228. [PubMed: 19614986]

Diez-Roux G, Banfi S, Sultan M, Geffers L, Anand S, Rozado D, Magen A, Canidio E, Pagani M, Peluso I, Lin-Marq N, Koch M, Bilio M, Cantiello I, Verde R, De Masi C, Bianchi SA, Cicchini J, Perroud E, Mehmeti S, Dagand E, Schrinner S, Nurnberger A, Schmidt K, Metz K, Zwingmann C, Brieske N, Springer C, Hernandez AM, Herzog S, Grabbe F, Sieverding C, Fischer B, Schrader K, Brockmeyer M, Dettmer S, Helbig C, Alunni V, Battaini MA, Mura C, Henrichsen CN, Garcia-Lopez R, Echevarria D, Puelles E, Garcia-Calero E, Kruse S, Uhr M, Kauck C, Feng G, Milyaev N, Ong CK, Kumar L, Lam M, Semple CA, Gyenesei A, Mundlos S, Radelof U, Lehrach H, Sarmientos P, Reymond A, Davidson DR, Dolle P, Antonarakis SE, Yaspo ML, Martinez S, Baldock RA, Eichele G, Ballabio A. A high-resolution anatomical atlas of the transcriptome in the mouse embryo. PLoS biology. 2011; 9:e1000582. [PubMed: 21267068]

Do MT, Kang SH, Xue T, Zhong H, Liao HW, Bergles DE, Yau KW. Photon capture and signalling by melanopsin retinal ganglion cells. Nature. 2009; 457:281–287. [PubMed: 19118382]

Do-Nascimento JL, Do-Nascimento RS, Damasceno BA, Silveira LC. The neurons of the retinal ganglion cell layer of the guinea pig: quantitative analysis of their distribution and size. Braz J Med Biol Res. 1991; 24:199–214. [PubMed: 1726652]

Doi M, Uji Y, Yamamura H. Morphological classification of retinal ganglion cells in mice. J Comp Neurol. 1995; 356:368–386. [PubMed: 7543910]

Dräger UC, Hofbauer A. Antibodies to heavy neurofilament subunit detect a subpopulation of damaged ganglion cells in retina. Nature. 1984; 309:624–626. [PubMed: 6203041]

Dräger UC, Olsen JF. Origins of crossed and uncrossed retinal projections in pigmented and albino mice. J Comp Neurol. 1980; 191:383–412. [PubMed: 7410600]

Dräger UC, Olsen JF. Ganglion cell distribution in the retina of the mouse. Invest Ophthalmol Vis Sci. 1981; 20:285–293. [PubMed: 6162818]

Duenker N. Transforming growth factor-beta (TGF-beta) and programmed cell death in the vertebrate retina. Int Rev Cytol. 2005; 245:17–43. [PubMed: 16125544]

Edqvist PH, Myers SM, Hallbook F. Early identification of retinal subtypes in the developing, pre-laminated chick retina using the transcription factors Prox1, Lim1, Ap2alpha, Pax6, Isl1, Isl2, Lim3 and Chx10. Eur J Histochem. 2006; 50:147–154. [PubMed: 16864127]

Elshatory Y, Deng M, Xie X, Gan L. Expression of the LIM-homeodomain protein Isl1 in the developing and mature mouse retina. J Comp Neurol. 2007; 503:182–197. [PubMed: 17480014]

Feng G, Mellor RH, Bernstein M, Keller-Peck C, Nguyen QT, Wallace M, Nerbonne JM, Lichtman JW, Sanes JR. Imaging neuronal subsets in transgenic mice expressing multiple spectral variants of GFP. Neuron. 2000; 28:41–51. [PubMed: 11086982]

Fischer D, Leibinger M. Promoting optic nerve regeneration. Prog Retin Eye Res. 2012; 31:688–701. [PubMed: 22781340]

Fukuda Y. A three-group classification of rat retinal ganglion cells: histological and physiological studies. Brain Res. 1977; 119:327–334. [PubMed: 830390]

Galindo-Romero C, Avilés-Trigueros M, Jiménez-López M, Valiente-Soriano FJ, Salinas-Navarro M, Nadal-Nicolás F, Villegas-Pérez MP, Vidal-Sanz M, Agudo-Barriuso M. Axotomy-induced retinal ganglion cell death in adult mice: quantitative and topographic time course analyses. Exp Eye Res. 2011; 92:377–387. [PubMed: 21354138]

Galindo-Romero C, Jiménez-López M, García-Ayuso D, Salinas-Navarro M, Nadal-Nicolás FM, Agudo-Barriuso M, Villegas-Pérez MP, Avilés-Trigueros M, Vidal-Sanz M. Number and spatial distribution of intrinsically photosensitive retinal ganglion cells in the adult albino rat. Exp Eye Res. 2013; 108:84–93. [PubMed: 23295345]

Galli-Resta L, Resta G, Tan SS, Reese BE. Mosaics of islet-1-expressing amacrine cells assembled by short-range cellular interactions. J Neurosci. 1997; 17:7831–7838. [PubMed: 9315903]

Gan WB, Grutzendler J, Wong WT, Wong RO, Lichtman JW. Multicolor “DiOlistic” labeling of the nervous system using lipophilic dye combinations. Neuron. 2000; 27:219–225. [PubMed: 10985343]

Gerber WV, Yatskievych TA, Antin PB, Correia KM, Conlon RA, Krieg PA. The RNA-binding protein gene, hermes, is expressed at high levels in the developing heart. Mech Dev. 1999; 80:77–86. [PubMed: 10096065]

Goldstein ME, Sternberger NH, Sternberger LA. Phosphorylation protects neurofilaments against proteolysis. J Neuroimmunol. 1987; 14:149–160. [PubMed: 3029175]

Hattar S, Liao HW, Takao M, Berson DM, Yau KW. Melanopsin-containing retinal ganglion cells: architecture, projections, and intrinsic photosensitivity. Science. 2002; 295:1065–1070. [PubMed: 11834834]

Haverkamp S, Inta D, Monyer H, Wässle H. Expression analysis of green fluorescent protein in retinal neurons of four transgenic mouse lines. Neuroscience. 2009; 160:126–139. [PubMed: 19232378]

Hirano AA, Brandstätter JH, Brecha NC. Cellular distribution and subcellular localization of molecular components of vesicular transmitter release in horizontal cells of rabbit retina. J Comp Neurol. 2005; 488:70–81. [PubMed: 15912504]

Hörnberg H, Holt C. RNA-binding proteins and translational regulation in axons and growth cones. Front Neurosci. 2013; 7:81. [PubMed: 23734093]

Hörnberg H, Wollerton-van Horck F, Maurus D, Zwart M, Svoboda H, Harris WA, Holt CE. RNA-binding protein Hermes/RBPMS inversely affects synapse density and axon arbor formation in retinal ganglion cells In Vivo. J Neurosci. 2013; 33:10384–10395. [PubMed: 23785151]

Huberman AD, Manu M, Koch SM, Susman MW, Lutz AB, Ullian EM, Baccus SA, Barres BA. Architecture and activity-mediated refinement of axonal projections from a mosaic of genetically identified retinal ganglion cells. Neuron. 2008; 59:425–438. [PubMed: 18701068]

Hughes A, Wieniawa-Narkiewicz E. A newly identified population of presumptive microneurones in the cat retinal ganglion cell layer. Nature. 1980; 284:468–470. [PubMed: 7360282]

Huxlin KR, Goodchild AK. Retinal ganglion cells in the albino rat: revised morphological classification. J Comp Neurol. 1997; 385:309–323. [PubMed: 9268130]

Inoue A, Obata K, Akagawa K. Cloning and sequence analysis of cDNA for a neuronal cell membrane antigen, HPC-1. J Biol Chem. 1992; 267:10613–10619. [PubMed: 1587842]

Ito T, Hioki H, Nakamura K, Tanaka Y, Nakade H, Kaneko T, Iino S, Nojyo Y. Gamma-aminobutyric acid-containing sympathetic preganglionic neurons in rat thoracic spinal cord send their axons to the superior cervical ganglion. J Comp Neurol. 2007; 502:113–125. [PubMed: 17335042]

Jain V, Ravindran E, Dhingra NK. Differential expression of Brn3 transcription factors in intrinsically photosensitive retinal ganglion cells in mouse. J Comp Neurol. 2012; 520:742–755. [PubMed: 21935940]

Jeon CJ, Strettoi E, Masland RH. The major cell populations of the mouse retina. J Neurosci. 1998; 18:8936–8946. [PubMed: 9786999]

Johansson UE, Eftekhari S, Warfvinge K. A battery of cell- and structure-specific markers for the adult porcine retina. J Histochem Cytochem. 2010; 58:377–389. [PubMed: 20086234]

Kao YH, Sterling P. Displaced GAD65 amacrine cells of the guinea pig retina are morphologically diverse. Vis Neurosci. 2006; 23:931–939. [PubMed: 17266785]

Kay JN, Voinescu PE, Chu MW, Sanes JR. Neurod6 expression defines new retinal amacrine cell subtypes and regulates their fate. Nat Neurosci. 2011; 14:965–972. [PubMed: 21743471]

Kim IJ, Zhang Y, Yamagata M, Meister M, Sanes JR. Molecular identification of a retinal cell type that responds to upward motion. Nature. 2008; 452:478–482. [PubMed: 18368118]

Kim TJ, Jeon CJ. Morphological classification of parvalbumin-containing retinal ganglion cells in mouse: single-cell injection after immunocytochemistry. Invest Ophthalmol Vis Sci. 2006; 47:2757–2764. [PubMed: 16799011]

Kong JH, Fish DR, Rockhill RL, Masland RH. Diversity of ganglion cells in the mouse retina: unsupervised morphological classification and its limits. J Comp Neurol. 2005; 489:293–310. [PubMed: 16025455]

Kong WC, Cho EY. Antibodies against neurofilament subunits label retinal ganglion cells but not displaced amacrine cells of hamsters. Life Sci. 1999; 64:1773–1778. [PubMed: 10353631]

Koontz MA, Hendrickson LE, Brace ST, Hendrickson AE. Immunocytochemical localization of GABA and glycine in amacrine and displaced amacrine cells of macaque monkey retina. Vis Res. 1993; 33:2617–2628. [PubMed: 8296457]

Kwong JM, Caprioli J, Piri N. RNA binding protein with multiple splicing: a new marker for retinal ganglion cells. Invest Ophthalmol Vis Sci. 2010; 51:1052–1058. [PubMed: 19737887]

Kwong JM, Quan A, Kyung H, Piri N, Caprioli J. Quantitative analysis of retinal ganglion cell survival with Rbpms immunolabeling in animal models of optic neuropathies. Invest Ophthalmol Vis Sci. 2011; 52:9694–9702. [PubMed: 22110060]

Lee ES, Lee JY, Jeon CJ. Types and density of calretinin-containing retinal ganglion cells in mouse. Neurosci Res. 2010; 66:141–150. [PubMed: 19895859]

Lin B, Wang SW, Masland RH. Retinal ganglion cell type, size, and spacing can be specified independent of homotypic dendritic contacts. Neuron. 2004; 43:475–485. [PubMed: 15312647]

Lind D, Franken S, Kappler J, Jankowski J, Schilling K. Characterization of the neuronal marker NeuN as a multiply phosphorylated antigen with discrete subcellular localization. J Neurosci Res. 2005; 79:295–302. [PubMed: 15605376]

Linden R. Displaced ganglion cells in the retina of the rat. J Comp Neurol. 1987; 258:138–143. [PubMed: 3571534]

Linden R, Perry VH. Ganglion cell death within the developing retina: a regulatory role for retinal dendrites? Neuroscience. 1982; 7:2813–2827. [PubMed: 7155355]

Liu X, Robinson ML, Schreiber AM, Wu V, Lavail MM, Cang J, Copenhagen DR. Regulation of neonatal development of retinal ganglion cell dendrites by neurotrophin-3 overexpression. J Comp Neurol. 2009; 514:449–458. [PubMed: 19350645]

Liu ZH, Jen LS. Displaced retinal ganglion cells in normal rats and rats with one eye enucleated at birth. Neurosci Lett. 1986; 67:239–244. [PubMed: 3737010]

Lunde BM, Moore C, Varani G. RNA-binding proteins: modular design for efficient function. Nat Rev Mol Cell Biol. 2007; 8:479–490. [PubMed: 17473849]

Maris C, Dominguez C, Allain FH. The RNA recognition motif, a plastic RNA-binding platform to regulate post-transcriptional gene expression. FEBS J. 2005; 272:2118–2131. [PubMed: 15853797]

Menger N, Pow DV, Wässle H. Glycinergic amacrine cells of the rat retina. J Comp Neurol. 1998; 401:34–46. [PubMed: 9802699]

Mullen RJ, Buck CR, Smith AM. NeuN, a neuronal specific nuclear protein in vertebrates. Development. 1992; 116:201–211. [PubMed: 1483388]

Munch TA, da Silveira RA, Siegert S, Viney TJ, Awatramani GB, Roska B. Approach sensitivity in the retina processed by a multifunctional neural circuit. Nat Neurosci. 2009; 12:1308–1316. [PubMed: 19734895]

Murali D, Kawaguchi-Niida M, Deng CX, Furuta Y. Smad4 is required predominantly in the developmental processes dependent on the BMP branch of the TGF-beta signaling system in the embryonic mouse retina. Invest Ophthalmol Vis Sci. 2011; 52:2930–2937. [PubMed: 21273545]

Nadal-Nicolás FM, Jiménez-López M, Salinas-Navarro M, Sobrado-Calvo P, Alburquerque-Béjar JJ, Vidal-Sanz M, Agudo-Barriuso M. Whole number, distribution and co-expression of brn3 transcription factors in retinal ganglion cells of adult albino and pigmented rats. PLoS One. 2012; 7:e49830. [PubMed: 23166779]

Nadal-Nicolás FM, Jiménez-López M, Sobrado-Calvo P, Nieto-Lopez L, Canovas-Martinez I, Salinas-Navarro M, Vidal-Sanz M, Agudo M. Brn3a as a marker of retinal ganglion cells: qualitative and quantitative time course studies in naive and optic nerve-injured retinas. Invest Ophthalmol Vis Sci. 2009; 50:3860–3868. [PubMed: 19264888]

Oyster CW, Takahashi ES, Hurst DC. Density, soma size, and regional distribution of rabbit retinal ganglion cells. J Neurosci. 1981; 1:1331–1346. [PubMed: 7320749]

Pan F, Paul DL, Bloomfield SA, Völgyi B. Connexin36 is required for gap junctional coupling of most ganglion cell subtypes in the mouse retina. J Comp Neurol. 2010; 518:911–927. [PubMed: 20058323]

Panda S, Sato TK, Castrucci AM, Rollag MD, DeGrip WJ, Hogenesch JB, Provencio I, Kay SA. Melanopsin (Opn4) requirement for normal light-induced circadian phase shifting. Science. 2002; 298:2213–2216. [PubMed: 12481141]

Pang JJ, Paul DL, Wu SM. Survey on amacrine cells coupling to retrograde-identified ganglion cells in the mouse retina. Invest Ophthalmol Vis Sci. 2013; 54:5151–5162. [PubMed: 23821205]

Pang JJ, Wu SM. Morphology and immunoreactivity of retrogradely double-labeled ganglion cells in the mouse retina. Invest Ophthalmol Vis Sci. 2011; 52:4886–4896. [PubMed: 21482641]

Panzanelli P, Fritschy JM, Yanagawa Y, Obata K, Sassoe-Pognetto M. GABAergic phenotype of periglomerular cells in the rodent olfactory bulb. J Comp Neurol. 2007; 502:990–1002. [PubMed: 17444497]

Pasteels B, Rogers J, Blachier F, Pochet R. Calbindin and calretinin localization in retina from different species. Vis Neurosci. 1990; 5:1–16. [PubMed: 2125465]

Peichl L, González-Soriano J. Unexpected presence of neurofilaments in axon-bearing horizontal cells of the mammalian retina. J Neurosci. 1993; 13:4091–4100. [PubMed: 8366362]

Pérez de Sevilla Müller L, Dedek K, Janssen-Bienhold U, Meyer A, Kreuzberg MM, Lorenz S, Willecke K, Weiler R. Expression and modulation of connexin 30.2, a novel gap junction protein in the mouse retina. Vis Neurosci. 2010a; 27:91–101. [PubMed: 20537217]

Pérez de Sevilla Müller L, Do MT, Yau KW, He S, Baldridge WH. Tracer coupling of intrinsically photosensitive retinal ganglion cells to amacrine cells in the mouse retina. J Comp Neurol. 2010b; 518:4813–4824. [PubMed: 20963830]

Pérez de Sevilla Müller L, Shelley J, Weiler R. Displaced amacrine cells of the mouse retina. J Comp Neurol. 2007; 505:177–189. [PubMed: 17853452]

Perry VH. Evidence for an amacrine cell system in the ganglion cell layer of the rat retina. Neuroscience. 1981; 6:931–944. [PubMed: 6165929]

Perry VH, Cowey A. Retinal ganglion cells that project to the superior colliculus and pretectum in the macaque monkey. Neuroscience. 1984; 12:1125–1137. [PubMed: 6483194]

Perry VH, Cowey A. The ganglion cell and cone distributions in the monkey's retina: implications for central magnification factors. Vis Res. 1985; 25:1795–1810. [PubMed: 3832605]

Perry VH, Morris RJ, Raisman G. Is Thy-1 expressed only by ganglion cells and their axons in the retina and optic nerve? J Neurocytol. 1984a; 13:809–824. [PubMed: 6210349]

Perry VH, Oehler R, Cowey A. Retinal ganglion cells that project to the dorsal lateral geniculate nucleus in the macaque monkey. Neuroscience. 1984b; 12:1101–1123. [PubMed: 6483193]

Perry VH, Walker M. Amacrine cells, displaced amacrine cells and interplexiform cells in the retina of the rat. Proc R Soc Lond B Biol Sci. 1980; 208:415–431. [PubMed: 6158054]

Piri N, Kwong JM, Song M, Caprioli J. Expression of hermes gene is restricted to the ganglion cells in the retina. Neurosci Lett. 2006; 405:40–45. [PubMed: 16870336]

Pow DV, Hendrickson AE. Distribution of the glycine transporter glyt-1 in mammalian and nonmammalian retinae. Vis Neurosci. 1999; 16:231–239. [PubMed: 10367958]

Pow DV, Wright LL, Vaney DI. The immunocytochemical detection of amino-acid neurotransmitters in paraformaldehyde-fixed tissues. J Neurosci Methods. 1995; 56:115–123. [PubMed: 7752677]

Quina LA, Pak W, Lanier J, Banwait P, Gratwick K, Liu Y, Velasquez T, O'Leary DD, Goulding M, Turner EE. Brn3a-expressing retinal ganglion cells project specifically to thalamocortical and collicular visual pathways. J Neurosci. 2005; 25:11595–11604. [PubMed: 16354917]

Raymond ID, Vila A, Huynh UC, Brecha NC. Cyan fluorescent protein expression in ganglion and amacrine cells in a thy1-CFP transgenic mouse retina. Mol Vis. 2008; 14:1559–1574. [PubMed: 18728756]

Remtulla S, Hallett PE. A schematic eye for the mouse, and comparisons with the rat. Vis Res. 1985; 25:21–31. [PubMed: 3984214]

Robson JA, Holländer H. Displaced ganglion cells in the rabbit retina. Invest Ophthalmol Vis Sci. 1984; 25:1376–1381. [PubMed: 6511223]

Rockhill RL, Daly FJ, MacNeil MA, Brown SP, Masland RH. The diversity of ganglion cells in a mammalian retina. J Neurosci. 2002; 22:3831–3843. [PubMed: 11978858]

Salinas-Navarro M, Jiménez-López M, Valiente-Soriano FJ, Alarcon-Martinez L, Avilés-Trigueros M, Mayor S, Holmes T, Lund RD, Villegas-Perez MP, Vidal-Sanz M. Retinal ganglion cell population in adult albino and pigmented mice: a computerized analysis of the entire population and its spatial distribution. Vis Res. 2009; 49:637–647. [PubMed: 19948111]

Sanna PP, Keyser KT, Battenberg E, Bloom FE. Parvalbumin immunoreactivity in the rat retina. Neurosci Lett. 1990; 118:136–139. [PubMed: 2259462]

Sargoy A, Sun X, Barnes S, Brecha NC. Differential calcium signalling mediated by voltage gated calcium channels in rat retinal ganglion cells and their unmyelinated axons. PLoS One. 2013 In Press.

Schindelin J, Arganda-Carreras I, Frise E, Kaynig V, Longair M, Pietzsch T, Preibisch S, Rueden C, Saalfeld S, Schmid B, Tinevez JY, White DJ, Hartenstein V, Eliceiri K, Tomancak P, Cardona A. Fiji: an open-source platform for biological-image analysis. Nat Methods. 2012; 9:676–682. [PubMed: 22743772]

Schubert T, Maxeiner S, Krüger O, Willecke K, Weiler R. Connexin45 mediates gap junctional coupling of bistratified ganglion cells in the mouse retina. J Comp Neurol. 2005; 490:29–39. [PubMed: 16041717]

Sherry DM, Mitchell R, Standifer KM, du Plessis B. Distribution of plasma membrane-associated syntaxins 1 through 4 indicates distinct trafficking functions in the synaptic layers of the mouse retina. BMC Neurosci. 2006; 7:54. [PubMed: 16839421]

Shimamoto A, Kitao S, Ichikawa K, Suzuki N, Yamabe Y, Imamura O, Tokutake Y, Satoh M, Matsumoto T, Kuromitsu J, Kataoka H, Sugawara K, Sugawara M, Sugimoto M, Goto M, Furuichi Y. A unique human gene that spans over 230 kb in the human chromosome 8p11–12

and codes multiple family proteins sharing RNA-binding motifs. Proc Natl Acad Sci U S A. 1996; 93:10913–10917. [PubMed: 8855282]

Sternberger LA, Sternberger NH. Monoclonal antibodies distinguish phosphorylated and nonphosphorylated forms of neurofilaments in situ. Proc Natl Acad Sci U S A. 1983; 80:6126–6130. [PubMed: 6577472]

Sun W, Li N, He S. Large-scale morophological survey of rat retinal ganglion cells. Vis Neurosci. 2002a; 19:483–493. [PubMed: 12511081]

Sun W, Li N, He S. Large-scale morphological survey of mouse retinal ganglion cells. J Comp Neurol. 2002b; 451:115–126. [PubMed: 12209831]

Sun Y, Ding L, Zhang H, Han J, Yang X, Yan J, Zhu Y, Li J, Song H, Ye Q. Potentiation of Smad-mediated transcriptional activation by the RNA-binding protein RBPMS. Nucleic Acids Res. 2006; 34:6314–6326. [PubMed: 17099224]

Templeton JP, Nassr M, Vazquez-Chona F, Freeman-Anderson NE, Orr WE, Williams RW, Geisert EE. Differential response of C57BL/6J mouse and DBA/2J mouse to optic nerve crush. BMC Neurosci. 2009; 10:90. [PubMed: 19643015]

Vaney DI. A quantitative comparison between the ganglion cell populations and axonal outflows of the visual streak and periphery of the rabbit retina. J Comp Neurol. 1980; 189:215–233. [PubMed: 7364963]

Vaney DI, Nelson JC, Pow DV. Neurotransmitter coupling through gap junctions in the retina. J Neurosci. 1998; 18:10594–10602. [PubMed: 9852595]

Villegas-Perez MP, Vidal-Sanz M, Rasminsky M, Bray GM, Aguayo AJ. Rapid and protracted phases of retinal ganglion cell loss follow axotomy in the optic nerve of adult rats. J Neurobiol. 1993; 24:23–36. [PubMed: 8419522]

Völgyi B, Chheda S, Bloomfield SA. Tracer coupling patterns of the ganglion cell subtypes in the mouse retina. J Comp Neurol. 2009; 512:664–687. [PubMed: 19051243]

Wang SW, Kim BS, Ding K, Wang H, Sun D, Johnson RL, Klein WH, Gan L. Requirement for math5 in the development of retinal ganglion cells. Genes Dev. 2001; 15:24–29. [PubMed: 11156601]

Wässle H, Boycott BB. Functional architecture of the mammalian retina. Physiol Rev. 1991; 71:447–480. [PubMed: 2006220]

Wässle H, Boycott BB, Illing RB. Morphology and mosaic of on- and off-beta cells in the cat retina and some functional considerations. Proc R Soc Lond B Biol Sci. 1981; 212:177–195. [PubMed: 6166013]

Wässle H, Chun MH, Muller F. Amacrine cells in the ganglion cell layer of the cat retina. J Comp Neurol. 1987; 265:391–408. [PubMed: 3693612]

Wässle H, Grünert U, Röhrenbeck J, Boycott BB. Retinal ganglion cell density and cortical magnification factor in the primate. Vis Res. 1990; 30:1897–1911. [PubMed: 2288097]

Williams RW, Strom RC, Rice DS, Goldowitz D. Genetic and environmental control of variation in retinal ganglion cell number in mice. J Neurosci. 1996; 16:7193–7205. [PubMed: 8929428]

Wilmore HP, McClive PJ, Smith CA, Sinclair AH. Expression profile of the RNA-binding protein gene hermes during chicken embryonic development. Dev Dyn. 2005; 233:1045–1051. [PubMed: 15895363]

Wolansky T, Pagliardini S, Greer JJ, Dickson CT. Immunohistochemical characterization of substance P receptor (NK(1)R)-expressing interneurons in the entorhinal cortex. J Comp Neurol. 2007; 502:427–441. [PubMed: 17366610]

Wordinger RJ, Clark AF. Bone morphogenetic proteins and their receptors in the eye. Exp Biol Med (Maywood). 2007; 232:979–992. [PubMed: 17720944]

Xiang M, Zhou L, Macke JP, Yoshioka T, Hendry SH, Eddy RL, Shows TB, Nathans J. The Brn-3 family of POU-domain factors: primary structure, binding specificity, and expression in subsets of retinal ganglion cells and somatosensory neurons. J Neurosci. 1995; 15:4762–4785. [PubMed: 7623109]

Zhang XM, Li Liu DT, Chiang SW, Choy KW, Pang CP, Lam DS, Yam GH. Immunopanning purification and long-term culture of human retinal ganglion cells. Mol Vis. 2010; 16:2867–2872. [PubMed: 21203402]

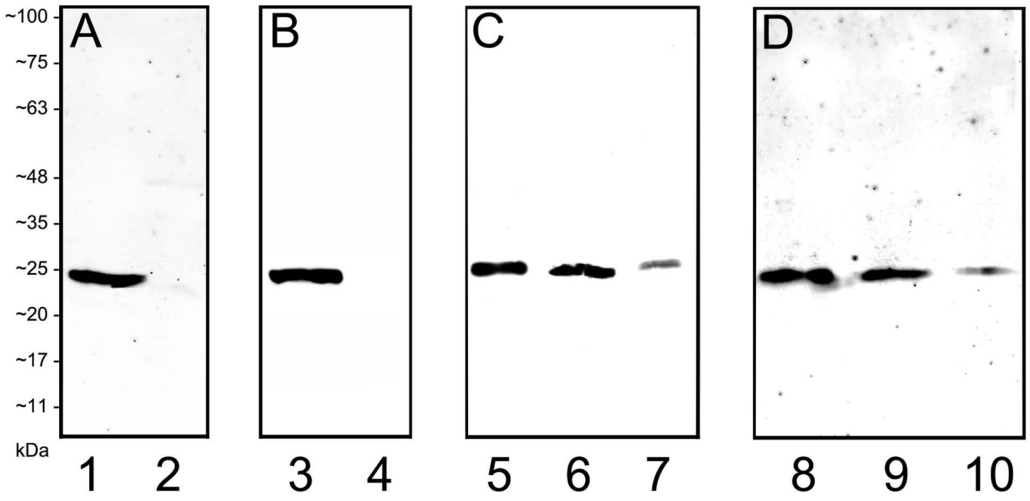

Figure 1.

Characterization of RBPMS antibodies and localization of RBPMS to the mouse and rat retina using Western blot analysis. The antibodies detected a single band at ~24 kDa corresponding to RBPMS in HEK293T cell lysates, and in mouse and rat retinal extracts. **A:** Guinea pig (GP15029) antibody; 10 μg of HEK293T cell lysates transfected with human RBPMS cDNA (lane 1) and control (lane 2). **B:** Rabbit (RB15027) antibody; 10 μg of HEK293T cell lysates, transfected with human RBPMS cDNA (lane 3) and control (lane 4). **C:** Guinea pig (GP15029) antibody; mouse retina (lane 5), rat retina (lane 6), and rat retina 56 days after optic nerve transection (lane 7); 25 μg homogenate each lane. **D:** Rabbit (RB15027) antibody; mouse retina (lane 8), rat retina (lane 9), and rat retina 56 days after optic nerve transection (lane 10); 25 μg homogenate each lane. Antibodies used at a dilution of 1:1000.

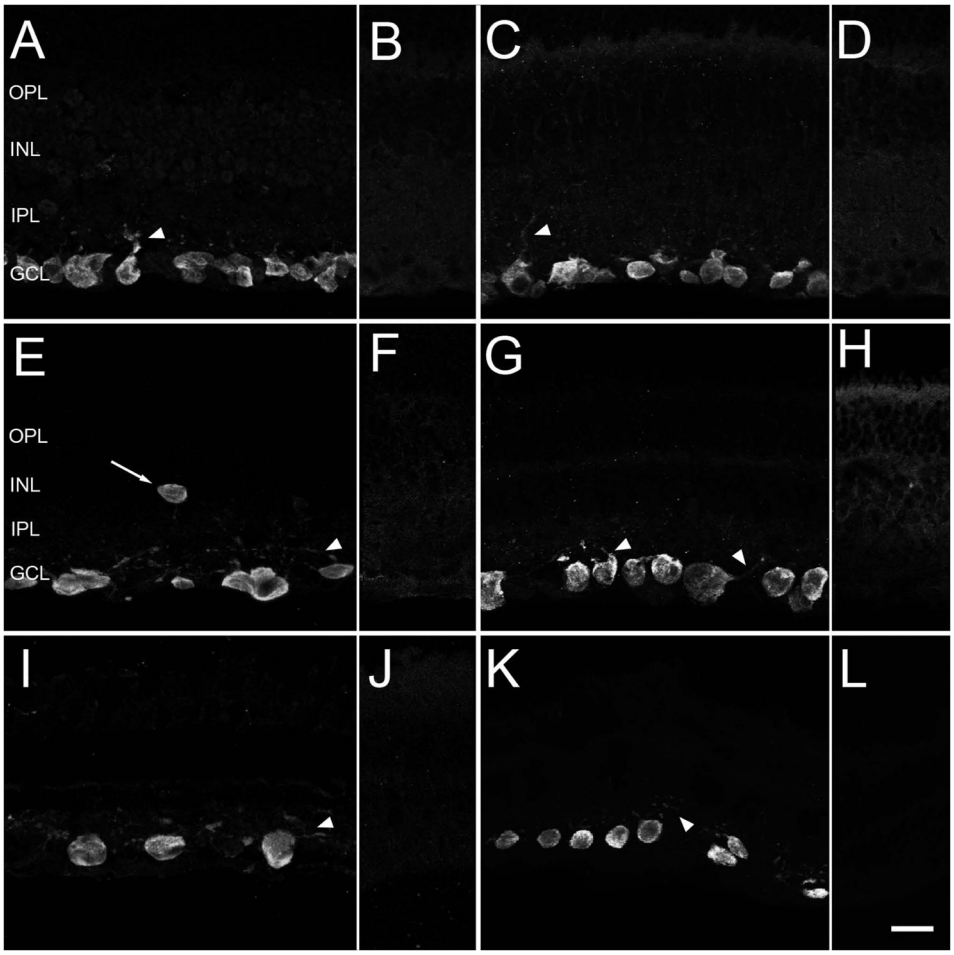

Figure 2.

Robust RBPMS immunoreactivity is primarily expressed by cell bodies located in the ganglion cell layer (GCL) of mouse, rat, guinea pig, rabbit and monkey retina. **A, C:** Mouse, **E:** Rat, **G:** Guinea pig, **I:** Rabbit, **K:** Monkey. Arrowheads indicate faintly immunostained primary dendrites. Arrow indicates a RBPMS immunoreactive cell in the inner nuclear layer (INL). **B, D, F, H, J, L:** Preabsorption control experiments with the RBPMS peptide fragment used for immunization showed a lack of immunostaining in mice, rat, guinea pig, rabbit and monkey retina. **A, B:** RBPMS rabbit antibody RB15027 and **C–L:** Guinea pig antibody GP15029. IPL, inner plexiform layer; OPL, outer plexiform layer. z-step = 0.55 μm. 10–14 optical sections were compressed for viewing. Scale bar = 20 μm.

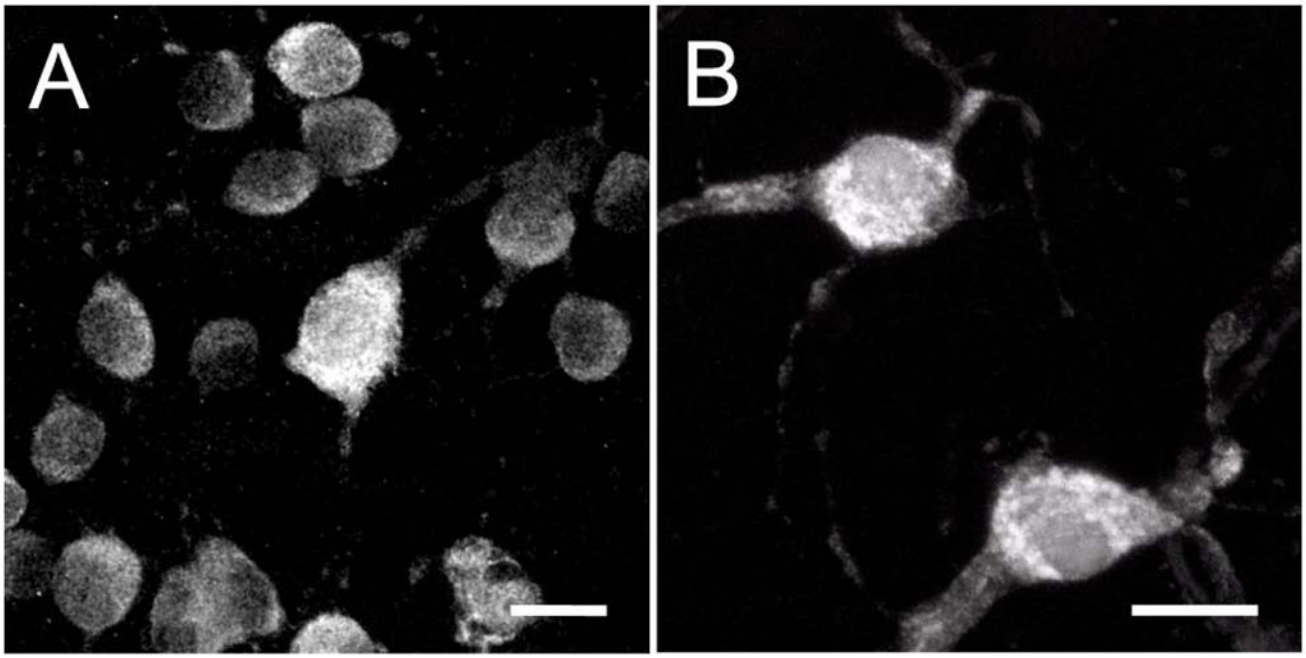

Figure 3.
RBPMS immunoreactivity is strongest in the somata, and weaker in primary and secondary dendrites. **A:** Peripheral mouse retina. **B:** Peripheral monkey retina. Plane of focus is at the GCL and includes the proximal IPL. z-step = 0.34–0.64 μm. 20 optical sections were compressed for viewing. RBPMS antibody GP15029. Scale bar = 20 μm.

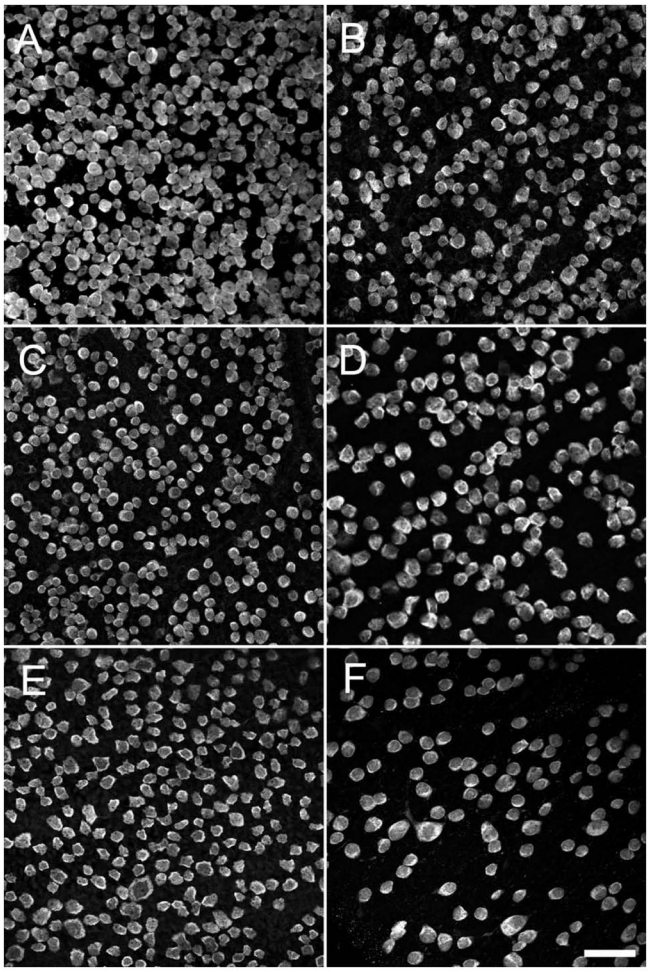

Figure 4.

RBPMS-immunoreactive cells in the GCL in whole-mount retinal preparations. **A:** Mouse, 1.5 mm from the optic nerve head. **B:** Mouse, 3 mm from the optic nerve head. **C:** Rat, 2 mm from the optic nerve head. **D:** Guinea pig, peripheral retina. **E:** Rabbit, mid peripheral retina. **F:** Monkey, far peripheral retina. z-step = 1.1 μm. 5–11 optical sections were compressed for viewing. RBPMS antibody GP15029. Scale bar = 50 μm.

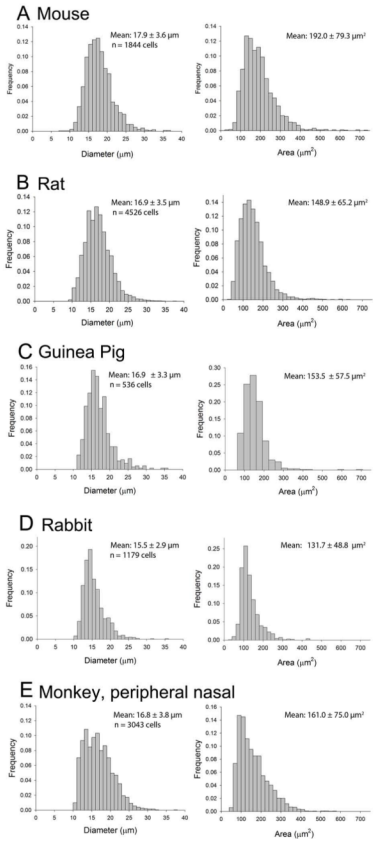

Figure 5.
Distribution of the cell diameters (left column) and areas (right column) of RBPMS-expressing cells in the GCL. **A:** Mouse. **B:** Rat. **C:** Guinea pig. **D:** Rabbit. **E:** Monkey. Mean ± SD.

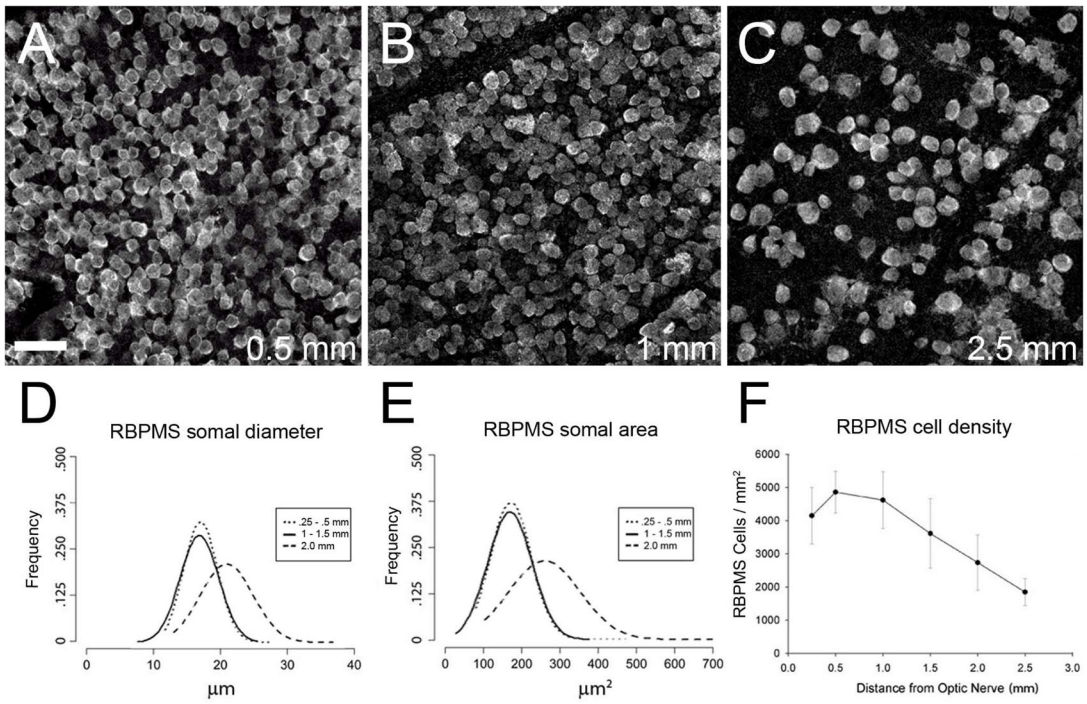

Figure 6.

Distribution of RBPMS cells in the mouse retina. **A–C:** Mouse GCL in a whole-mount at 0.5, 1.0 and 2.5 mm from the optic nerve head, respectively. **D:** Frequency of RBPMS somal diameters in central (dotted line, solid line) and peripheral retina (dashed line). **E:** Frequency of RBPMS somal areas in central (dotted line, solid line) and peripheral retina (dashed line). **F:** RBPMS cell density vs. distance from the optic nerve head (N=4 retinas). z-step = 1.1 μm. 11 optical sections were compressed for viewing. RBPMS antibody GP15029. Scale bar = 50 μm.

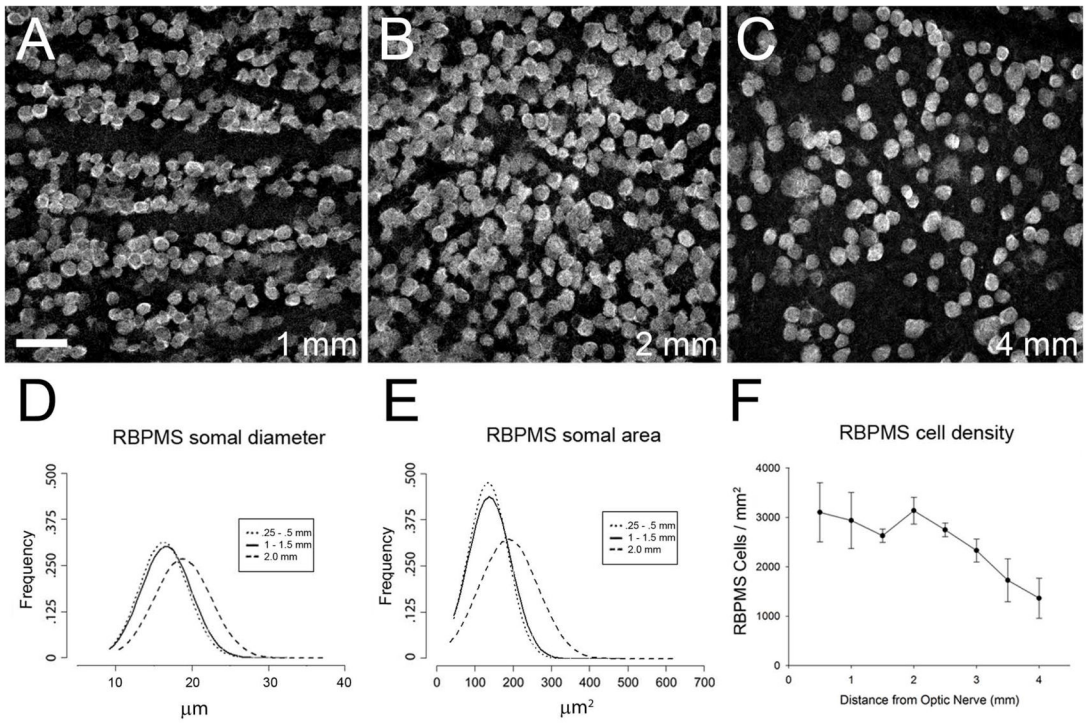

Figure 7.

Distribution of RBPMS cells in rat retina. **A–C:** Rat GCL in a whole-mount at 1, 2, and 4 mm from the optic nerve head, respectively. **D:** Frequency of RBPMS somal diameters in central (dotted line, solid line) and peripheral retina (dashed line). **E:** Frequency of RBPMS areas in central (dotted line, solid line) and peripheral retina (dashed line). **F:** RBPMS cell density vs. distance from the optic nerve head (N=4 retinas). z-step = 1.1 μm. 11 optical sections were compressed for viewing. RBPMS antibody GP15029. Scale bar = 50 μm.

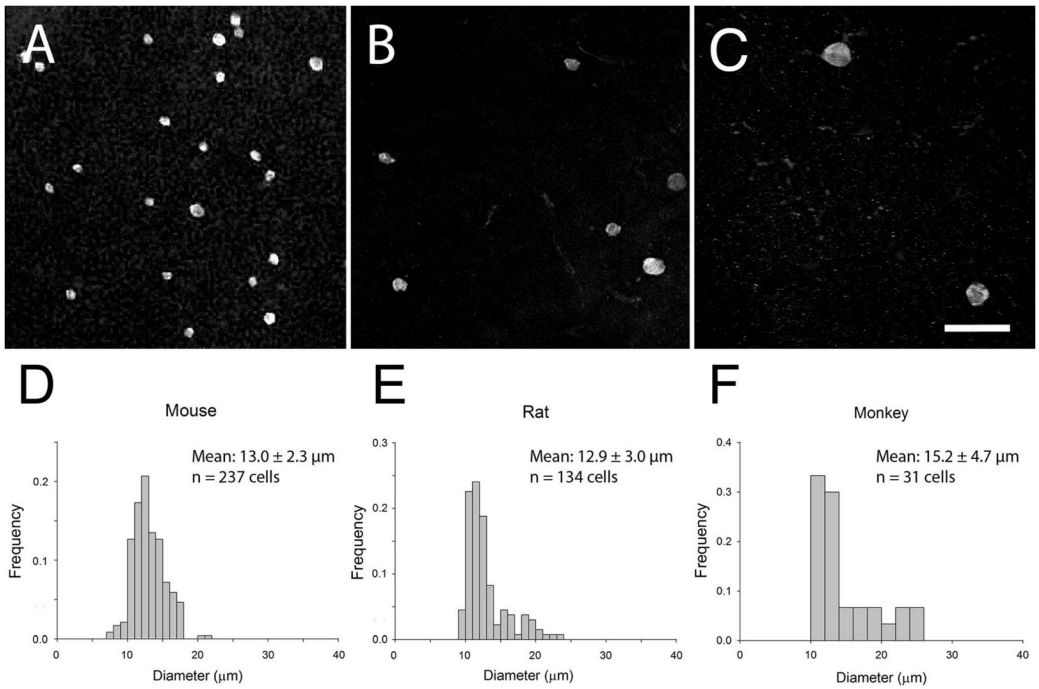

Figure 8.

Sparsely distributed RBPMS-immunoreactive cells were located in the proxmal INL. **A:** Mouse. **B:** Rat. **C:** Monkey. **D–F:** Frequency and mean size of RBPMS somal diameters in the INL. RBPMS-immunoreactive cells were observed in all retinal regions, mainly in the peripheral retina. z-step = 0.8–1.0 μm. 11–24 optical sections were compressed for viewing. Mean ± SD. RBPMS antibody GP15029. Scale bar = 50 μm.

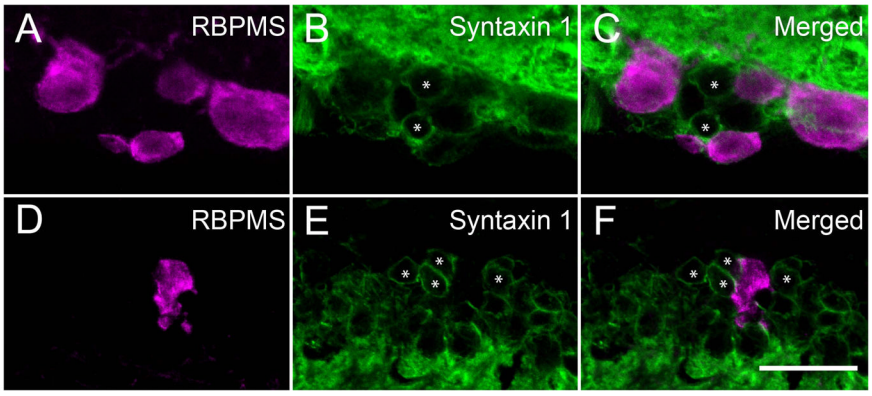

Figure 9.

Amacrine cells did not contain RBPMS immunoreactivity. RBPMS immunoreactivity was not detected in displaced amacrine cells in the GCL and amacrine cells in the INL identified by syntaxin1 (HPC-1) immunoreactivity in the mouse retina (* marks displaced amacrine and amacrine cells). GCL; **A:** RBPMS. **B:** Syntaxin1. **C:** Merged image. INL; **D:** RBPMS. **E:** Syntaxin1. **F:** Merged image. Vertical retinal sections. z-step = 0.5 μm. 15 optical sections were compressed for viewing. RBPMS antibody GP15029. Scale bar = 20 μm.

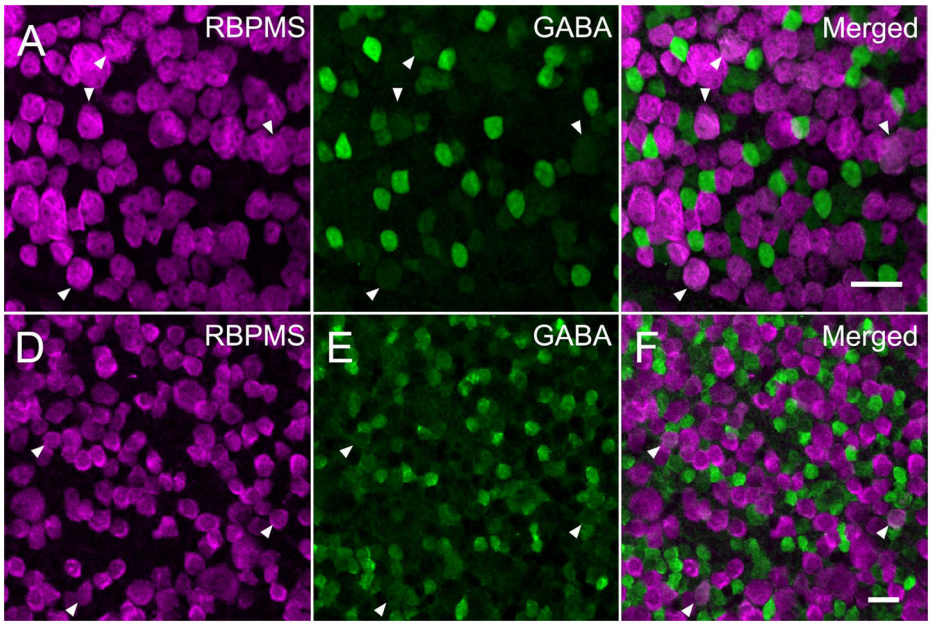

Figure 10.

RBPMS immunoreactivity was not expressed in most GABA-containing cells in the mouse and rat GCL. GABA immunoreactivity was expressed in displaced amacrine cells in whole-mounted mouse (**A–C**) and rat (**D–F**) retina. About 5% of the RBPMS cells contained weak GABA immunoreactivity in mouse and rat retina, respectively. Arrowheads indicate cells containing both RBPMS immunoreactivity and weak GABA immunoreactivity. **A, D:** RBPMS. **B, E:** GABA. **C, F:** merged image. Plane of focus in GCL. z-step = 0.65–1.1 μm. 9 optical sections were compressed for viewing. RBPMS antibody GP15029. Scale bar = 20 μm.

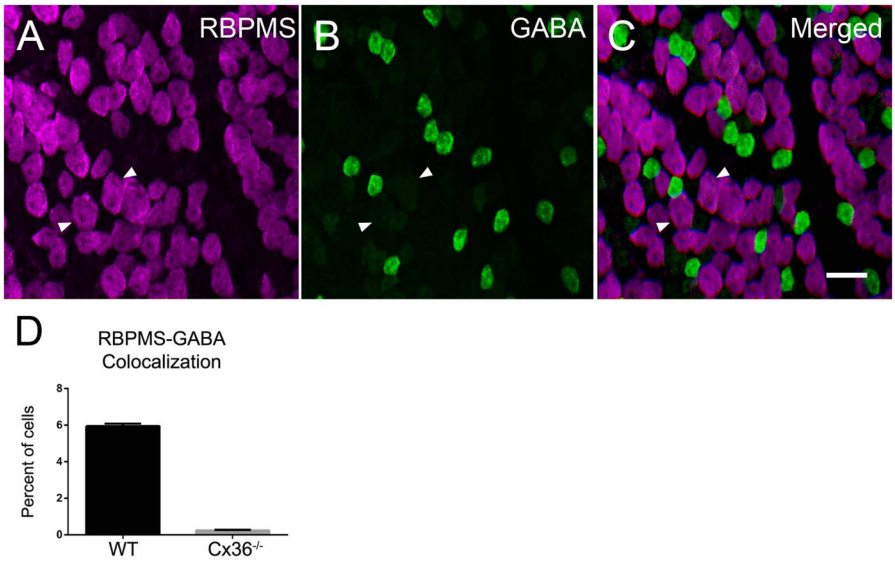

Figure 11.

The majority of RBPMS cells in the Cx36$^{-/-}$ mouse retina did not contain GABA immunoreactivity (**A–D**), although there were a few RBPMS cells with weak GABA immunoreactivity. Arrowheads indicate cells containing both RBPMS and weak GABA immunoreactivity. **A:** RBPMS. **B:** GABA. **C:** Merged image. **D:** Percentage of cells expressing both RBPMS and GABA immunoreactivity in wild-type (WT) and Cx36$^{-/-}$ whole-mounted retinas. Three wild-type (WT) and Cx36$^{-/-}$ retinas were evaluated. Plane of focus in GCL. z-step = 0.65 μm. 9 optical sections were compressed for viewing. RBPMS antibody GP15029. Scale bar = 20 μm.

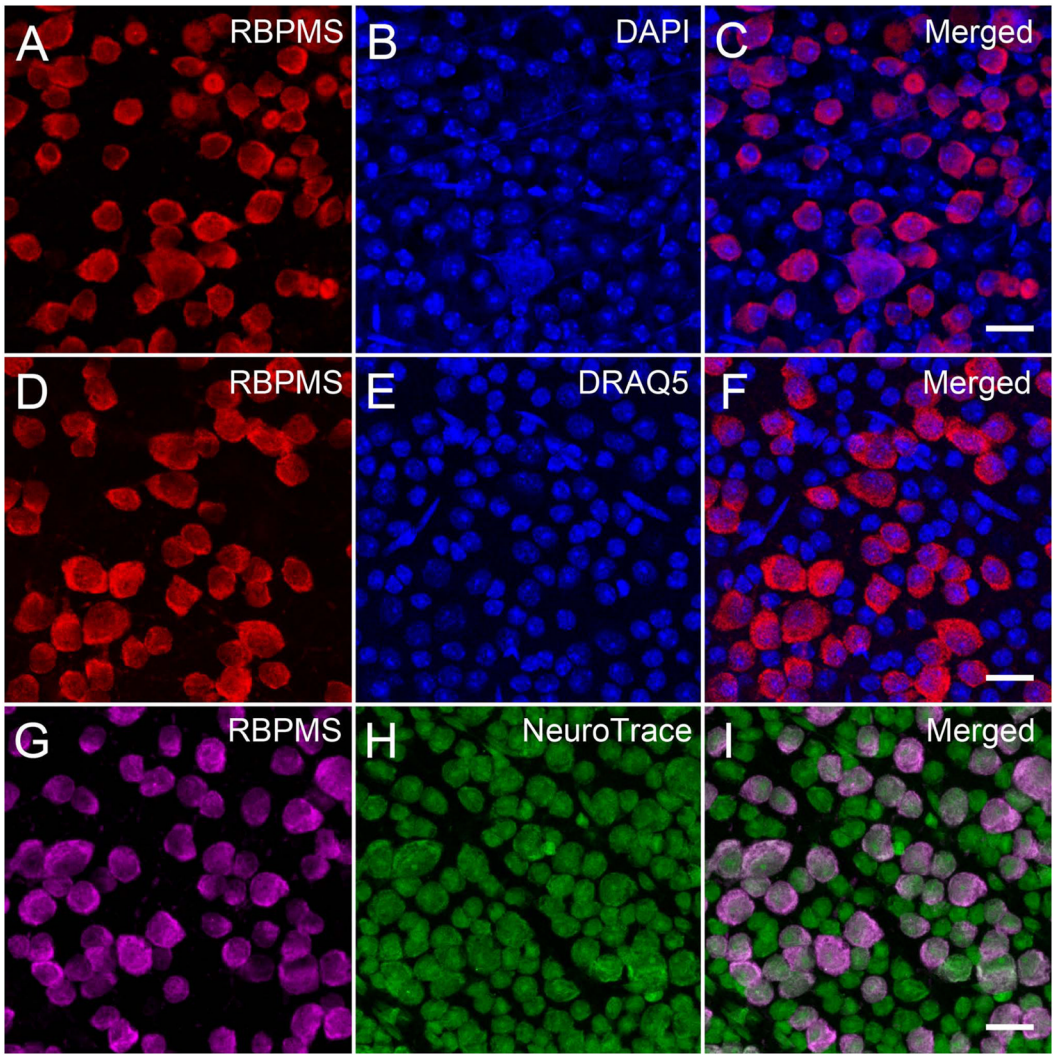

Figure 12.

RBPMS immunoreactivity was mainly expressed in medium and large somata in the mouse GCL. Mouse whole-mounted retinas immunostained with RBPMS antibodies and counterstained with DAPI, DRAQ5 or NeuroTrace. DAPI and DRAQ5 labeled all nuclei, and NeuroTrace labeled RGC and displaced amacrine cell somata in the GCL. **A, D, G:** RBPMS. **B:** DAPI. **E:** DRAQ5. **H:** NeuroTrace. **C, F, I:** Merged images. Plane of focus in GCL for all images. z-step = 0.97 μm. 8 optical sections were compressed for viewing. RBPMS antibody GP15029. Scale bar = 20 μm.

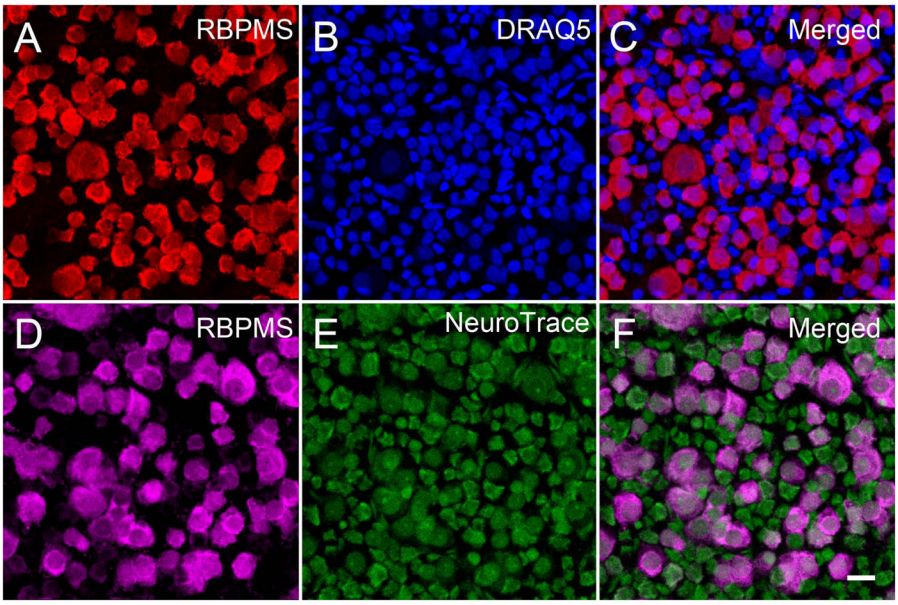

Figure 13.

RBPMS immunoreactivity was mainly expressed in medium and large cells in the rat GCL. Rat whole-mounted retinas immunostained with RBPMS antibodies and counterstained with DRAQ5 or NeuroTrace. DRAQ5 stained all nuclei, and NeuroTrace stained RGC and displaced amacrine cell bodies. **A, D:** RBPMS. **B:** DRAQ5. **E:** NeuroTrace. **C, F:** Merged images. Plane of focus in GCL for all images. z-step = 0.51 μm. 13 optical sections were compressed for viewing. RBPMS antibody GP15029. Scale bar = 20 um.

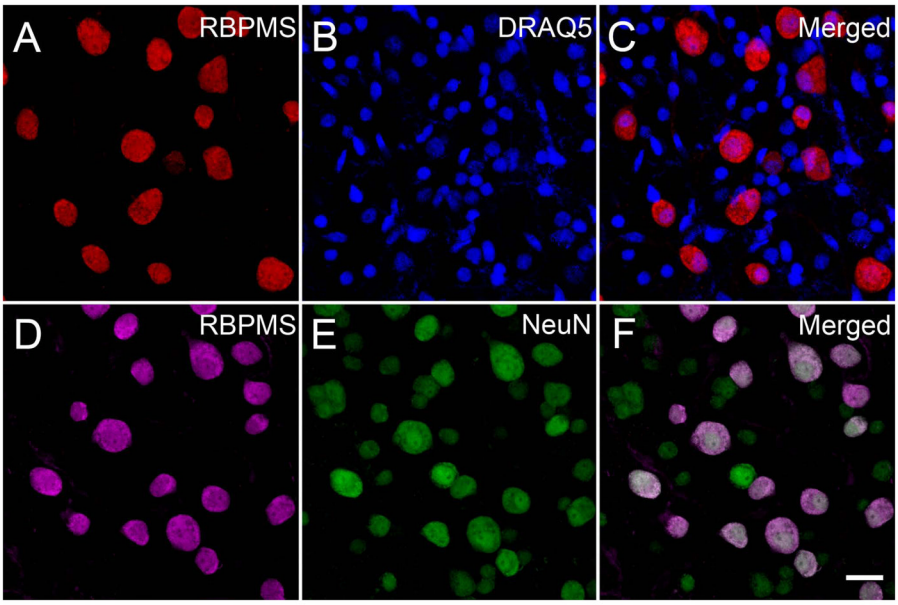

Figure 14.

RBPMS immunoreactivity was mainly expressed in medium and large cells in the monkey GCL. Monkey whole-mounted retinas immunostained with RBPMS antibodies and counterstained with DRAQ5 or NeuN antibodies. DRAQ5 labeled all nuclei, and NeuN immunoreactivity was expressed in the nucleus and cytoplasm of RGC and displaced amacrine cell somata. Note that there was a greater number of small DRAQ5 stained nuclei than small diameter NeuN immunoreactive cells at the same retinal eccentricity, suggesting NeuN is expressed by some, but not all displaced amacrine cells. **A, D:** RBPMS. **B:** DRAQ5. **E:** NeuN. **C, F:** Merged images. Both sets of images are from the same peripheral retinal location. Plane of focus in GCL for all images. z-step = 0.47 μm. 8 optical sections were compressed for viewing. RBPMS antibody GP15029. Scale bar = 20 μm.

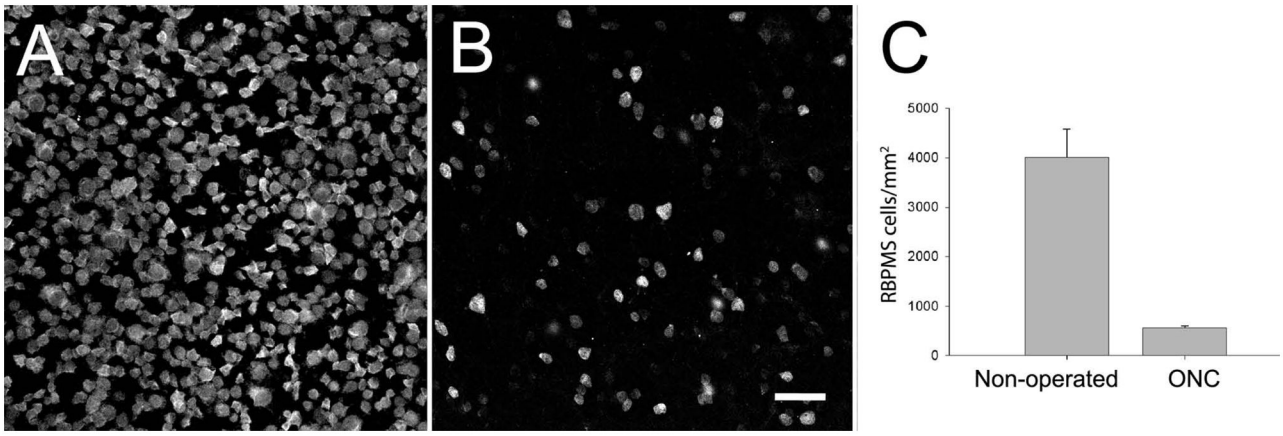

Figure 15.

RBPMS-immunoreactive cells in the GCL of the mouse retina following unilateral optic nerve crush (ONC). **A:** GCL of the contralateral, non-operated retina. **B:** GCL of the ONC retina. **C:** RBPMS cell density in the central retina is markedly reduced 21 days after ONC compared to the non-operated retina. The retinas from 4 non-operated and 4 ONC eyes were analyzed. z-step = 0.6 μm. 7–9 optical sections were compressed for viewing. RBPMS antibody GP15029. Scale bar = 50 μm.

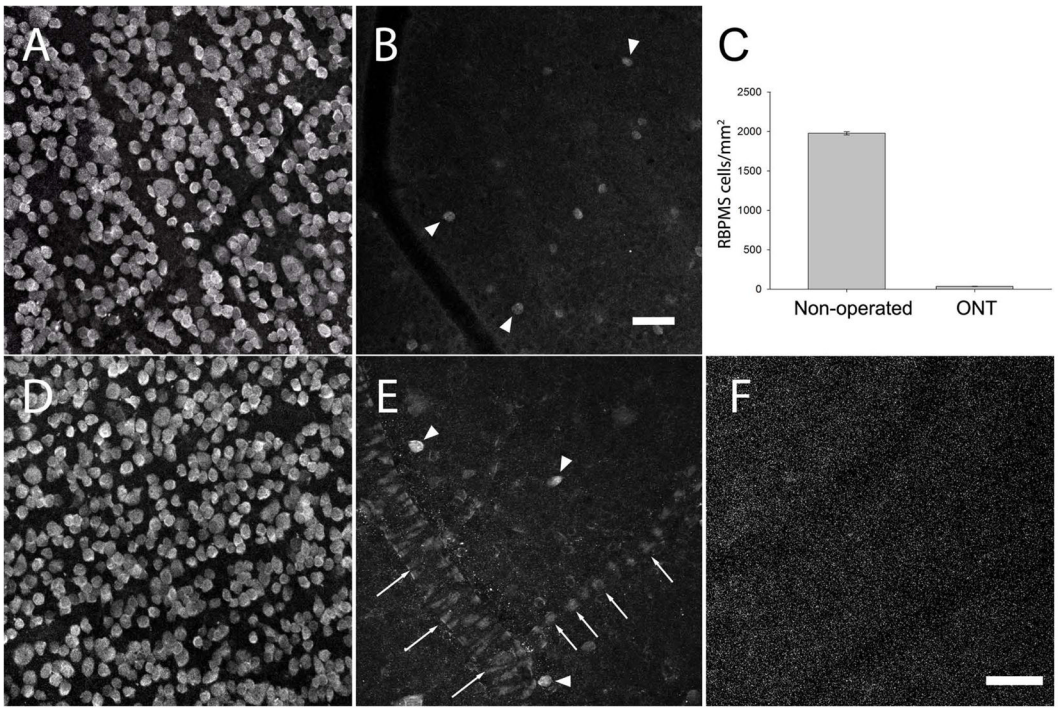

Figure 16.

RBPMS-immunoreactive cells in the GCL of the rat retina following unilateral optic nerve transection (ONT). **A:** GCL of the contralateral, non-operated retina. **B:** GCL of an axotomized retina 21 days after ONT (arrowheads indicate RBPMS immunoreactive cells). **C:** RBPMS cell density in the GCL decreased ~98% compared to the non-operated retina. RBPMS cell density was determined in 3 non-operated and 3 ONT eyes. **D:** GCL of the non-operated retina used as the control for the study illustrated in E and F. **E:** GCL of an axotomized retina 21 days after ONT (arrowheads indicate RBPMS cells). Note weak RBPMS immunostaining by endothelial cells of the blood vessels. **F:** RBPMS antibody preabsorbed with RBPMS immunizing peptide blocks immunolabeling of all cells including endothelial cells in the ONT retina. z-step = 1.1 μm. 12–14 optical sections were compressed for viewing. RBPMS antibody GP15029. Scale bar = 50 μm.

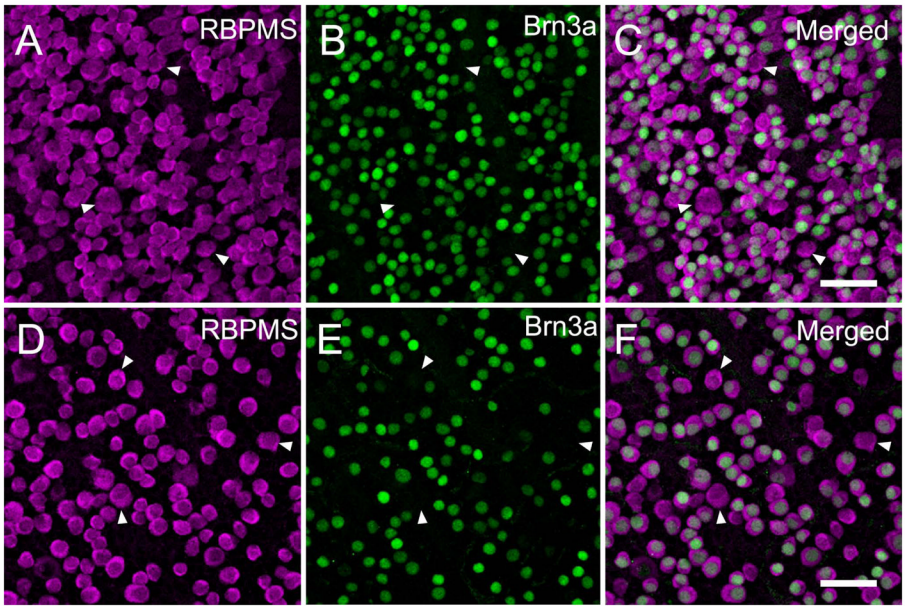

Figure 17.

Co-expression of the RGC marker, Brn3a and RBPMS in mouse and rat retina. All Brn3a immunoreactive cells contained RBPMS immunoreactivity, and conversely about 80% of the RBPMS cells in the GCL contain Brn3a immunoreactivity. Arrowheads indicate cells with RBPMS immunoreactivity that lack Brn3a immunoreactive nuclei. Mouse retina; **A:** RBPMS. **B:** Brn3a. **C:** Merged image. Rat retina; **D**: RBPMS. **E**: Brn3a. **F**: Merged image. Plane of focus in GCL for all images. z-step = 1.1 μm. 10 optical sections were compressed for viewing. RBPMS antibody GP15029. Scale bar = 50 μm.

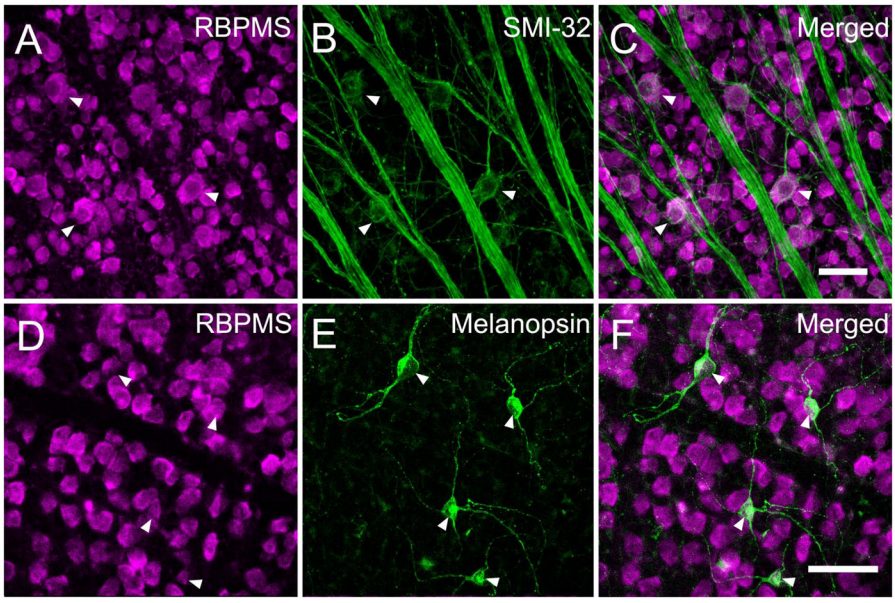

Figure 18.

Co-expression of the RGC markers, SMI-32 or melanopsin with RBPMS in the rat retina. Arrowheads indicate ganglion cells expressing RBPMS immunoreactivity and SMI-32 or melanopsin immunoreactivity. **A:** RBPMS **B:** SMI-32. **C:** Merged image. **D:** RBPMS. **E:** Melanopsin. **F:** Merged image. Retinal whole-mount. Plane of focus in GCL for all images. z-step = 1.0 μm. 9 optical sections were compressed for viewing. RBPMS antibody GP15029. Scale bar = 50 μm.

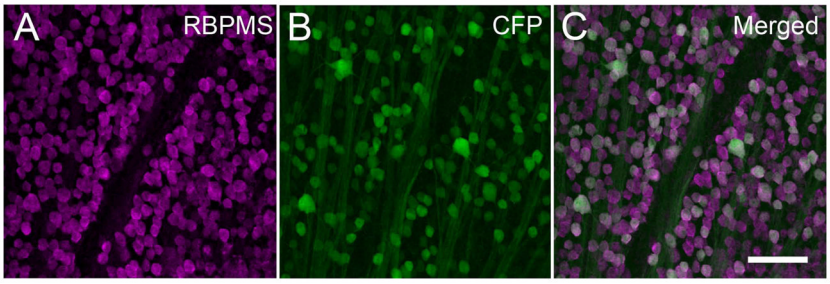

Figure 19.

Co-expression of Thy1-CFP fluorescence with RBPMS in the mouse retina. Thy1-CFP fluorescence is predominatly expressed in RGCs. Arrowheads indicate fluorescent cells containing RBPMS immunoreactivity. **A:** RBPMS. **B:** Thy1-CFP fluorescence in the GCL. **C:** Merged image. Plane of focus in GCL for all images. RBPMS antibody GP15029. z-step = 1.1 μm. 10 optical sections were compressed for viewing. Scale bar = 50 μm.

Table 1

Primary Antibodies

Antibody	Antigen/immunogen	Species, dilution	Source, catalog No.
RBPMS	$RBPMS_{4-24}$ with N-terminal cys; GGKAEKENTPSEANLQEEEVRC- KLH conjugate	Rabbit & Guinea Pig affinity purified polyclonal; 1:1000–5000 (after dilution to 0.01 μg/μl)	Present study; GP15029-3, GP15029-F RB15027-3, RB15027-F
Brn3a	$Brn3a_{186-224}$-T7 gene10 protein	Mouse monoclonal; 1:1000	EMD Millipore; MAB1585
GABA	GABA-bovine serum albumin conjugate	Rabbit polyclonal; 1:500	Sigma; A2052
Glycine	Glycine-thyroglobulin conjugate	Rat polyclonal; 1:1000	ImmunoSolution; IG1002
Melanopsin	Mouse melanopsin; N-terminal 15 amino acids*	Rabbit polyclonal; 1:5000	Advanced Targeting Systems; UF006
Melanopsin	Rat $melanopsin_{455-474}$; QKSKTPKTKRHLPSLDRRM-M–thyroglobulin conjugate	Rabbit polyclonal; 1:250	Thermo Scientific; PA-781
NeuN	Purified cell nuclei from mouse brain	Mouse monoclonal; 1:500	Chemicon; MAB377B
SMI-32	Non-phosphorylated epitopes on the medium and heavy molecular weight subunits of neurofilament H	Mouse monoclonal; 1:500	Sternberger Monoclonals Incorporated; Lot #17; SMI-32
Syntaxin 1	synaptosomal plasma membrane fraction of rat hippocampus	Mouse monoclonal; 1:5000	Sigma; clone HPC-1; S0664

*Vendor did not provide additional information

Table 2

RBPMS somal size

	Ganglion cell layer				Inner nuclear layer			
	Diameter (μm)		Area (μm^2)		Diameter (μm)		Area (μm^2)	
	Mean ± SD	Median	Mean ± SD	Median	Mean ± SD	Median	Mean ± SD	Median
Mouse	17.9 ± 3.6	17.4	192.0 ± 79.3	178.5	13.0 ± 2.3	12.7	104.6 ± 37.3	98.0
Rat	16.9 ± 3.5	16.6	148.9 ± 65.2	138.8	12.9 ± 3.0	11.9	141.2 ± 81.3	149.0
Guinea Pig	16.9 ± 3.3	15.9	150.7 ± 54.2	139.9	13.3 ± 2.3	12.6	155.5 ± 46.0	148.0
Rabbit	15.5 ± 2.9	14.8	131.7 ± 48.8	119.2	16.5 ± 2.4	16.4	138.6 ± 21.6	124.3
*Monkey	12.7 ± 2.5	12.7	89.9 ± 33.1	88.2	12.4 ± 1.6	12.2	80.4 ± 19.0	80.4
**Monkey	16.8 ± 3.8	16.1	161.0 ± 75.0	143.5	20.3 ± 4.3	20.5	283.9 ± 65.0	212.0

* Monkey; central - temporal retina

** Monkey; nasal inferior retina

Table 3

Comparison of RBPMS and RGC somal sizes in the GCL

	Range	Mean ± SD	Labeling	Reference
Mouse	7.4 to 36.8 μm; 60 to 735 μm^2	17.9 ± 3.6 μm; 192.0 ± 79.63 μm^2	RBPMS immunoreactivity	This paper
	~30 to ~320 μm^2	NR	Nissl staining and HRP retrograde transport	(Dräger and Olsen, 1981)
	~50 to ~450 μm^2	113 ± 47 μm^2 (contra) 153 ± 84 μm^2 (ipsi)	HRP retrograde transport	(Dräger and Olsen, 1980) C57/BL6J mouse
	7 to 33 μm	NR	DiI biolistic delivery	(Sun et al., 2002b)
	~65 to ~575 μm^2	NR	DiI biolistic delivery, LY intracellular injections, YFP expression, antibody labeling	(Coombs et al., 2006)
	6 to 24 μm	NR	Neurobiotin and LY retrograde transport	(Pang and Wu, 2011)
Rat	9.1 to 37.4 μm	16.9 ± 3.5 μm	RBPMS immunoreactivity	This paper
	6 to 22 μm	11.1 μm (median)	HRP retrograde transport	(Linden, 1987)
	12 to 39 μm	NR	DiI retrograde transport	(Huxlin and Goodchild, 1997)
	8 to 32 μm	NR	DiI biolistic delivery	(Sun et al., 2002a)
Guinea pig	11.4 to 35.8 μm	16.9 ± 3.3 μm	RBPMS immunoreactivity	This paper
	<10 to >20 μm	12.55 μm	HRP retrograde transport	(Do-Nascimento et al., 1991)
Rabbit	10.1 to 36.0 μm	15.5 ± 2.9 μm	RBPMS immunoreactivity	This paper
	10 to 33 μm	18.8 μm	HRP retrograde transport	(Robson and Holländer, 1984)
	NR	12.1 μm; visual streak 15.5 μm; peripheral retina	Nissl staining	(Vaney, 1980)
Monkey	10.6 to 37.2 μm	16.8 ± 3.3 μm	RBPMS immunoreactivity	This paper; inferior nasal retina
	8 to 20+ μm	NR	HRP retrograde transport	(Bunt et al., 1975)
	10 to 25 μm, > 25 μm	NR	HRP retrograde transport (LGN*)	(Perry et al., 1984)
	~7 to 20 μm	NR	HRP retrograde transport (SC**)	(Perry and Cowey, 1984)

NR – not reported; Ipsi – ipsilateral; contra – contralateral;

* LGN – lateral geniculate nucleus;

** SC – superior colliculus

Table 4

Comparison of RBPMS and dRGC somal sizes in the INL

	Range	Mean ± SD	Labeling	Reference
Mouse	7.4 to 21.4 μm	13.0 ± 2.3 μm 104.6 ± 37.3 μm^2	RBPMS immunoreactivity	This paper
	~50 to 300 μm^2	132 ± 59 μm^2 (ipsi)	HRP retrograde transport	(Dräger and Olsen, 1980) C57/BL6J mouse
	<13 μm 13 to 17.5 μm >17.5	13–17.5 μm (most)	Neurobiotin and Lucifer yellow retrograde transport	(Pang and Wu, 2011)
Rat	9.1 to 23.0 μm	12.9 ± 3.0 μm	RBPMS immunoreactivity	This paper
	9 to 15.5	NR	HRP retrograde transport	(Perry, 1981)
	7 to 18 μm	NR	HRP retrograde transport	(Linden, 1987)
	8 to 19 μm	12 ± 2.8 μm	Fast Blue retrograde transport and Lucifer Yellow labeling	(Buhl and Dann, 1988)
Guinea pig	10.3 to 17.1 μm	13.3 ± 2.3 μm	RBPMS immunoreactivity	This paper
Rabbit	11.7 to 20.4 μm	16.5 ± 2.4 μm	RBPMS immunoreactivity	This paper
	10 to 17.7 μm	14.9 μm	HRP retrograde transport	(Robson and Holländer, 1984)
Monkey	13.3 to 27.3 μm	20.3 ± 4.3 μm	RBPMS immunoreactivity	This paper
	10 to 13 μm 15 to 25 μm	NR	HRP retrograde transport	(Bunt and Minckler, 1977)
	10 to 13 μm	NR	HRP retrograde transport	(Bunt et al., 1975)

NR – not reported; ipsi = ipsilateral